

# Fluid-Particle Drag in Low-Reynolds-Number Polydisperse Gas–Solid Suspensions

Xiaolong Yin and Sankaran Sundaresan

Chemical Engineering Dept., Princeton University, Princeton, NJ 08543

DOI 10.1002/aic.11800

Published online May 6, 2009 in Wiley InterScience (www.interscience.wiley.com).

*Lattice-Boltzmann simulations of low-Reynolds-number fluid flow in bidisperse fixed beds and suspensions with particle–particle relative motions have been performed. The particles are spherical and are intimately mixed. The total volume fraction of the suspension was varied between 0.1 and 0.4, the volume fraction ratio  $\phi_1/\phi_2$  from 1:1 to 1:6, and the particle size ratio  $d_1/d_2$  from 1:1.5 to 1:4. A drag law with improved accuracy has been established for bidisperse fixed beds. For suspensions with particle–particle relative motions, the hydrodynamic particle–particle drag representing the momentum transfer between particle species through hydrodynamic interaction is found to be an important contribution to the net fluid-particle drag. It has a logarithmic dependence on the lubrication cutoff distance and can be fit as the harmonic mean of the drag forces in bidisperse fixed beds. The proposed drag laws for bidisperse fixed beds and suspensions are generalized to polydisperse suspensions with three or more particle species. © 2009 American Institute of Chemical Engineers *AIChE J*, 55: 1352–1368, 2009*

*Keywords: fluid-particle drag, gas-solid suspensions, low reynolds number, polydisperse, particle size distribution*

## Introduction

Gas–solid suspensions are involved in many chemical engineering operations. When simulating gas–solid suspension flows in large containers, as it is impossible to solve the Navier-Stokes equations for the fluid and the equations of motion for all the particles, the particles and the fluid are usually modeled as two or more inter-penetrating continua, the dynamics of which are governed by locally averaged equations (Euler-Euler approach). For suspensions with much fewer particles, one can also track the positions and velocities of all particles in an explicit manner and model the fluid phase as the only continuum (Euler-Lagrangian approach). In either approach, the model equations rely on various constitutive relations to account for the many unknown terms emerging from averaging—fluid-particle drag, added-mass, lift, history force, and particle and fluid phase stresses. Among all these terms, the fluid-particle drag is particularly important for gas–solid suspensions: it is usu-

ally the primary force to suspend and transport the particles; it has a significant influence on the bed expansion and stability of the suspension. In the past, closures for fluid-particle drag were generally based on experimental measurements, and were largely empirical in nature; in recent years, however, drag laws generated from direct numerical simulations have become available, and it was shown in several case studies that the drag law has a significant influence over the qualitative and quantitative nature of the flow,<sup>1,2</sup> and computationally generated drag laws in many occasions can indeed improve the accuracy of the continuum simulation.<sup>3,4</sup> To date, most of the computationally generated drag laws were derived from flows past fixed, random assemblies of spheres of the same size<sup>5–7</sup> or two different sizes.<sup>8–10</sup> Even though these drag formulas have been adapted in ad hoc ways to study the dynamics of mono- and polydisperse gas–solid suspensions, it should be emphasized that freely evolving suspensions are different from fixed beds in that the particles move constantly, and an accurate drag law should consider the effect of particle velocity fluctuation when the Reynolds number of the particles is not small,<sup>11</sup> and the effect of particle–particle relative motion when the suspension of interest contains particles of different densities and/or sizes. Among

Correspondence concerning this article should be addressed to S. Sundaresan at [sundar@princeton.edu](mailto:sundar@princeton.edu).

these challenges, the effect of polydispersity is particularly interesting, because suspensions with particle size distributions are very common, and one can vary the amount of “fines” to control the flow characteristics of a gas-fluidized bed.<sup>12–17</sup> In a previous study, we characterized by direct numerical simulations the fluid-particle drag in a special type of polydisperse suspension containing equally sized spheres with particle–particle relative motion.<sup>18</sup> It was found that particle–particle relative motion gave rise to a hydrodynamic particle–particle drag term that forms an important part of the total fluid-particle drag; in this study, we consider more general polydisperse fixed beds and suspensions containing spheres of different sizes. Our parameter space encompasses a total volume fraction range of  $0.1 < \phi < 0.4$ , in which the volume fraction ratio  $\phi_1/\phi_2$  was varied from 1:1 to 1:6, and the particle size ratio  $d_1/d_2$  from 1:1.5 to 1:4. We first revisit bidisperse fixed beds and propose a more accurate drag formula. Then, assisted by the new formula developed for fixed beds, we develop a fitting function for the hydrodynamic particle–particle drag and propose a drag law for low-Reynolds-number polydisperse suspensions with particle–particle relative motion.

In this study, we focus on suspensions with low Reynolds numbers  $Re = \rho_g U d / \mu$  and large Stokes numbers  $St = (2\rho_p/9\rho_g)Re$ . Here  $\rho_g$  and  $\rho_p$  are densities of the fluid and the particles, respectively,  $U$  is a characteristic velocity describing particle-fluid relative motion,  $d$  is a length scale for particle size, and  $\mu$  is the viscosity of the fluid. Such a dual limit is realistic for many gas-particle systems of practical interest, e.g. 50–100  $\mu\text{m}$  particles suspended in air; it is also attractive in that it allows for efficient characterization of the drag forces. First, low-Reynolds-number flows are quasi-steady, allowing us to characterize the drag forces as a function of particle positions and velocities. In addition, the drag forces are linear functions of average particle velocities and are independent of the velocity fluctuations.<sup>11,18</sup> One can thus assume that particles of the same type have identical velocities and simplify the setup of simulations. It is valid to compute the forces as functions of particle positions and velocities for gas–solid suspensions with high Stokes numbers, because in such suspensions the fluid-particle force on a particle usually does not balance the weight of the particle due to the long relaxation time; the velocities of particles are more readily changed by collisions and obey Gaussian distributions.<sup>19,20</sup> In contrast, when particle Stokes number is low, which is less common for gas–solid suspensions but a reality for many liquid–solid colloidal suspensions, as the relaxation time is very short, a particle would adjust its velocity very quickly such that the fluid-particle force always balances its own weight. In this limit, it is more appropriate to use the fluid-particle forces as input parameters, and use mobility matrices or hindered settling functions to relate the velocities of particles to the forces. For discussions on mobility matrices or hindered settling functions, see Batchelor,<sup>21</sup> Batchelor and Wen,<sup>22</sup> Davis and Gecol,<sup>23</sup> and Revay and Higdon.<sup>24</sup>

This article is arranged in the following order. We will first define the fluid-particle drag in the context of averaged continua equations for gas–solid suspensions, and discuss existing computationally generated drag formulas for mono- and polydisperse suspensions. We will then introduce the lattice-Boltzmann method and the setup of the simulations.

After that, we present the drag forces in bidisperse fixed beds and propose a drag formula with improved accuracy. It is then followed by a study on suspensions with particle–particle relative motions. Assisted by the fixed-bed drag formula developed in this study, we were able to condense the volume fraction and particle size dependence of the drag forces obtained from simulations with particle–particle relative motion into a simple explicit drag formula that can easily be generalized to suspensions containing three or more particle species.

## Fluid-Particle Drag in Mono- and Polydisperse Gas–Solid Suspensions

### Drag in the context of averaged equations

The Euler-Euler approach for monodisperse gas–solid suspensions treat the particles and the interstitial gas as two interpenetrating continua. The averaged equations governing the dynamics of the suspension are discussed in many publications, e.g., Jackson,<sup>25</sup> and they can be easily generalized to multifluid model equations to describe polydisperse gas–solid suspensions.<sup>26,27</sup> Assuming that our suspension of interest contains two different types of particles and there is neither aggregation nor breakup of particles, we can write down the continuity equation for the gas phase

$$\frac{\partial((1-\phi)\rho_g)}{\partial t} + \nabla \cdot ((1-\phi)\rho_g \mathbf{U}_g) = 0, \quad (1)$$

and those for the particle phases ( $i = 1$  and  $2$ )

$$\frac{\partial(\phi_i \rho_i)}{\partial t} + \nabla \cdot (\phi_i \rho_i \mathbf{U}_i) = 0. \quad (2)$$

In Eqs. 1 and 2,  $\rho_g$  and  $\mathbf{U}_g$  are the density and average velocity of the gas phase,  $\phi_i$ ,  $\rho_i$ , and  $\mathbf{U}_i$  are the volume fraction, density, and average velocity of the  $i$ -th particle species.  $\phi = \sum_{i=1}^2 \phi_i$ . The averaged momentum equation for the gas phase is

$$\begin{aligned} \frac{\partial((1-\phi)\rho_g \mathbf{U}_g)}{\partial t} + \nabla \cdot ((1-\phi)\rho_g \mathbf{U}_g \mathbf{U}_g) \\ = \nabla \cdot \mathbf{S}_g - \sum_{i=1}^2 \mathbf{f}_{g-i} + (1-\phi)\rho_g \mathbf{g}. \end{aligned} \quad (3)$$

The momentum equations for the particle phases are

$$\begin{aligned} \frac{\partial(\phi_i \rho_i \mathbf{U}_i)}{\partial t} + \nabla \cdot (\phi_i \rho_i \mathbf{U}_i \mathbf{U}_i) = \nabla \cdot \mathbf{S}_i + \mathbf{f}_{g-i} \\ + \sum_{j=1, j \neq i}^2 \mathbf{f}_{j-i} + \phi_i \rho_i \mathbf{g}. \end{aligned} \quad (4)$$

In Eqs. 3 and 4,  $\mathbf{S}_g$  and  $\mathbf{S}_i$  are the stress tensors for the gas and the particle phases;  $\mathbf{f}_{g-i}$  represent the interactive forces per unit volume of suspension between the gas and the  $i$ -th particle phase;  $\mathbf{f}_{j-i}$  represent the interactive forces per unit volume of suspension between particles of phase  $j$  and particles of phase  $i$  due to collisions and/or enduring

contacts; finally,  $\mathbf{g}$  is the gravity.  $\mathbf{S}_g$  is usually expressed as  $-\mathbf{PI} + \tau_g$  with  $P$  the pressure in the gas phase and  $\tau_g$  the deviatoric stress. To solve Eqs. 1 through 4, one needs to supply constitutive models for  $\tau_g$ ,  $\mathbf{f}_{g-i}$ ,  $\mathbf{S}_i$ , and  $\mathbf{f}_{j-i}$ .

Closures for  $\mathbf{S}_i$  and  $\mathbf{f}_{j-i}$  for high Stokes number systems are often sought through kinetic theories. Alternative simulation methods, such as the Euler-Lagrange approach (e.g. Feng et al.<sup>28</sup> and Beetstra et al.<sup>4</sup>) or the Multi-Phase Particle-in-Cell (MP-PIC) method (e.g. Snider,<sup>29</sup> Leboireiro et al.<sup>2</sup>), circumvent the need to solve the particle phase averaged equations by tracking the motions of particles or “clouds” of particles using Newton’s equations of motion. Nevertheless, they still need constitutive models to account for the fluid-particle interaction  $\mathbf{f}_{g-i}$ . In general, a complete description of  $\mathbf{f}_{g-i}$  includes contributions from a variety of sources: the drag force  $\mathbf{f}_{Dg-i}$  resulting from the relative velocity between the fluid and the particles, the added mass force associated with the current relative acceleration, the history effect associated with the past history of relative acceleration, the generalized buoyancy, and the lift force, etc. As our simulations feature steady, low-Re flows with no bulk velocity gradient, the total fluid-particle force  $\mathbf{f}_{g-i}$  only contains the drag  $\mathbf{f}_{Dg-i}$  and the generalized buoyancy force  $-\phi_i \nabla P$

$$\mathbf{f}_{g-i} = -\phi_i \nabla P + \mathbf{f}_{Dg-i}. \quad (5)$$

Drag defined this way is consistent with the majority of chemical engineering literature. It should be noted, however, that the work by Hill et al.<sup>5,6</sup> considered the entire  $\mathbf{f}_{g-i}$  as the drag and did not subtract the bulk pressure gradient  $-\phi_i \nabla P$ . The readers should be aware of this difference when comparing expressions for drag forces from different sources.

### Computationally generated drag laws for low-Re fixed beds

For monodisperse suspensions, the constitutive relations for the fluid-particle drag  $\mathbf{f}_{Dg-i}$  are usually expressed as

$$\mathbf{f}_{D-\text{fixed}} = -\beta \Delta \mathbf{U}, \quad (6)$$

where  $\Delta \mathbf{U} = (\mathbf{U} - \mathbf{U}_g)$  is the average slip velocity between particles and the fluid, and  $\beta$  is the volume-specific friction coefficient. In Eq. 6, we replaced the subscript  $Dg-i$  with  $D - \text{fixed}$  to emphasize that it is for fixed beds with only one particle species. In addition, we placed a negative sign before  $\beta_i$  to reflect the fact that the drag force is in the opposite direction of  $\Delta \mathbf{U}$  and to make  $\beta$  positive. There exists several formulas for  $\beta$  that are based on direct numerical simulations of flow past fixed assemblies of spheres, e.g., Hill et al.<sup>5,6</sup> Koch and Hill,<sup>30</sup> Benyahia et al.<sup>7</sup> van der Hoef et al.<sup>8,9</sup> and Beetstra et al.<sup>10</sup> As the focus of this study is low-Re flows, here we pick among others the formula

$$\begin{aligned} F_{D-\text{fixed}}^* &= -\frac{F_{D-\text{fixed}}}{3\pi d \mu (1-\phi) \Delta U} \\ &= \frac{10\phi}{(1-\phi)^2} + (1-\phi)^2 (1 + 1.5\sqrt{\phi}) \end{aligned} \quad (7)$$

developed by van der Hoef et al.<sup>8</sup> for low-Re monodisperse fixed beds to compute  $F_{D-\text{fixed}}^*$ , the dimensionless average drag

force per particle. It is easy to show that  $\beta$  is proportional to  $F_{D-\text{fixed}}^*$  by

$$\beta = \frac{18\phi(1-\phi)\mu}{d^2} F_{D-\text{fixed}}^*. \quad (8)$$

For bidisperse fixed beds, each particle species would have its own drag correlation

$$\mathbf{f}_{Di-\text{fixed}} = -\beta_i \Delta \mathbf{U}. \quad (9)$$

Because of the added complexity due to particle size ratio  $d_1/d_2$  and volume fraction ratio  $\phi_1/\phi_2$ , developing a closure for  $\beta_i$  in bidisperse fixed beds is very difficult, and it is only recently that van der Hoef et al.<sup>8,9</sup> were able to establish the first computationally based closure for  $\beta_i$ . In their study, it was recognized that the average drag per particle for phase  $i$ ,  $F_{Di-\text{fixed}}$ , once properly normalized, can be expressed as a simple function of  $F_{D-\text{fixed}}^*$ , the drag in a monodisperse fixed bed of the same total volume fraction. The normalization procedure for  $F_{Di-\text{fixed}}$  is as follow. First, a dimensionless drag force for phase  $i$  is defined

$$F_{Di-\text{fixed}}^* = -\frac{F_{Di-\text{fixed}}}{3\pi d_i \mu (1-\phi) \Delta U}. \quad (10)$$

Then, by using the Sauter mean diameter

$$\langle d \rangle = \frac{n_1 d_1^3 + n_2 d_2^3}{n_1 d_1^2 + n_2 d_2^2} \quad (11)$$

where  $n_i$  is the number density of phase  $i$  particles, a dimensionless particle size  $y_i = d_i/\langle d \rangle$  is introduced. The numerical data by van der Hoef et al.<sup>8,9</sup> indicate that the ratio  $F_{Di-\text{fixed}}^*/F_{D-\text{fixed}}^*$  can be well approximated by simple functions of the total volume fraction  $\phi$  and the dimensionless size  $y_i$ . Van der Hoef et al.<sup>8,9</sup> proposed to use

$$F_{Di-\text{fixed}}^* = y_i F_{D-\text{fixed}}^* \quad (12)$$

as the first-order approximation of their numerical data. Note that Eq. 12 is different from the original expression in van der Hoef et al.<sup>8</sup> because of a later published erratum.<sup>9</sup> As in polydisperse fixed beds  $f_{Di-\text{fixed}} = n_i F_{Di-\text{fixed}}$ , it is easy to show that  $\beta_i$  is related to  $F_{Di-\text{fixed}}^*$  by

$$\beta_i = \frac{18\phi_i(1-\phi)\mu}{d_i^2} F_{Di-\text{fixed}}^*. \quad (13)$$

We will see later that even though Eq. 12 is not very accurate for bidisperse fixed beds with large particle size ratios, the idea that  $F_{Di-\text{fixed}}^*/F_{D-\text{fixed}}^*$  may be fit by simple functions of  $\phi$  and  $y_i$  provides an excellent foundation for the construction of more accurate formulas. It is worth pointing out that for fixed beds with large particle size ratios, van der Hoef et al.<sup>8</sup> suggested to modify Eq. 12 with  $O(y_i^3)$  corrections to improve the quality of fitting

$$\begin{cases} F_{D1-\text{fixed}}^*/F_{D-\text{fixed}}^* &= y_1 + 0.064y_1^3 \left(1 - \phi_1 - \phi_2 \frac{d_2}{d_1}\right) \\ F_{D2-\text{fixed}}^*/F_{D-\text{fixed}}^* &= y_2 + 0.064y_2^3 \left(1 - \phi_1 \frac{d_1}{d_2} - \phi_2\right) \end{cases} \quad (14)$$

The right-hand-side of Eq. 14, unlike Eq. 12, is no longer a simple function of  $y_i$  and  $\phi$ .

### Drag correlations for low-Re polydisperse gas–solid suspensions

Owing to the growing interest in the dynamics of polydisperse gas–solid suspensions, in particular, segregation and mixing, there have been a number of computational studies on polydisperse gas–solid suspensions in the past few years.<sup>2–4,27,28,31–36</sup> These studies employed ad hoc modifications of existing drag formulas with a general form

$$\mathbf{f}_{Di} = -\beta_i \Delta \mathbf{U}_i. \quad (15)$$

In this equation,  $\Delta \mathbf{U}_i = (\mathbf{U}_i - \mathbf{U}_g)$  is the average velocity of particle phase  $i$  relative to the fluid. Equation 15 implies that the drag acting on species  $i$  is independent of the velocities of other particle species, which is not physically sound for polydisperse suspensions with particle–particle relative motion because the presence of one particle species affects the motion of other species not only by changing the total solid fraction, but also through collisional and hydrodynamical particle–particle momentum transfer. In many Euler–Euler models, the particle phase momentum equations contain particle–particle drag terms to account for direct particle–particle collisions, e.g. Syamlal<sup>37</sup> and Huilin et al.<sup>38</sup> The indirect particle–particle momentum transfer mediated by the interstitial fluid, or the hydrodynamic particle–particle drag, being an integrated part of the net fluid-particle drag, is not included in such drag models.

In order to assess the importance of the hydrodynamic particle–particle drag, we would like to develop a drag law that includes not only the velocity of species  $i$  but also the velocities of other species. For bidisperse suspensions with relative velocities  $\Delta \mathbf{U}_1$  and  $\Delta \mathbf{U}_2$  aligned in the same direction, we can use a scalar drag law of the following form

$$\begin{cases} F_{D1} &= -B_{11} \Delta U_1 - B_{12} \Delta U_2 \\ F_{D2} &= -B_{21} \Delta U_1 - B_{22} \Delta U_2 \end{cases}, \quad (16)$$

where  $F_{Di}$  is the average drag force per particle of type  $i$ , and  $B_{ij}$  is the particle-specific friction coefficient of a bidisperse suspension. The influence on the drag of particle phase  $i$  due to the motion of particle phase  $j$  is reflected in the off-diagonal components of the matrix. Multiplying Eq. 16 by the number densities of particles, one can obtain the drag forces per unit volume of suspension

$$\begin{cases} f_{D1} &= -\beta_{11} \Delta U_1 - \beta_{12} \Delta U_2 \\ f_{D2} &= -\beta_{21} \Delta U_1 - \beta_{22} \Delta U_2 \end{cases}. \quad (17)$$

Here  $f_{Di} = n_i F_{Di}$ , and  $\beta_{ij} = n_i B_{ij}$  is the volume-specific friction coefficient of a bidisperse suspension.

In the aforementioned drag laws for fixed beds, the drag forces are nondimensionalized using the Stokes drag of an isolated particle (c.f. Eq. 10); in polydisperse suspensions, as there are more than one velocity scales available, it is best to nondimensionalize Eq. 16 using  $F_{Di}^* = \rho_g F_{Di} / \mu^2$  and  $B_{ij}^* = B_{ij} / \mu \langle d \rangle$

$$\begin{cases} F_{D1}^* &= -B_{11}^* \Delta \text{Re}_1 - B_{12}^* \Delta \text{Re}_2 \\ F_{D2}^* &= -B_{21}^* \Delta \text{Re}_1 - B_{22}^* \Delta \text{Re}_2 \end{cases}; \quad (18)$$

Equation 17 can be nondimensionalized using  $f_{Di}^* = \rho_g \langle d \rangle^3 f_{Di} / \mu^2$  and  $\beta_{ij}^* = \langle d \rangle^2 \beta_{ij} / \mu$

$$\begin{cases} f_{D1}^* &= -\beta_{11}^* \Delta \text{Re}_1 - \beta_{12}^* \Delta \text{Re}_2 \\ f_{D2}^* &= -\beta_{21}^* \Delta \text{Re}_1 - \beta_{22}^* \Delta \text{Re}_2 \end{cases}. \quad (19)$$

In the above two equations, the Reynolds numbers are defined as  $\Delta \text{Re}_i = \rho_g \Delta U_i \langle d \rangle / \mu$ . In our previous study,<sup>18</sup> we characterized the friction coefficients  $B_{ij}^*$  and  $\beta_{ij}^*$  for bidisperse suspensions of equally sized spheres with particle–particle relative motion, i.e.,  $d_1 = d_2$  and  $\Delta U_1 \neq \Delta U_2$ . It was found that the off-diagonal components of the friction coefficient matrix are always important, and the size of the off-diagonals is influenced by the intensity of the lubrication interaction between particles. In this study, we use numerical simulations to characterize  $B_{ij}^*$  and  $\beta_{ij}^*$  for bidisperse suspensions of unequally sized spheres, and develop formulas to fit them.

### Simulation Method and Setup

The numerical method used in this work is the Susp3D lattice-Boltzmann program developed by Ladd<sup>39,40</sup> for suspensions of spherical particles. It has been modified and improved over the years, and a complete review is available in Ladd and Verberg.<sup>41</sup> This program has been used to study many particle-laden flow problems, including the aforementioned studies on fluid-particle drag by Hill et al.<sup>5,6</sup> van der Hoef et al.<sup>8</sup> Beetstra et al.<sup>10</sup> and Yin and Sundaresan.<sup>18</sup> Because detailed information of this method are well available in the literature, here we will only provide a brief description.

The lattice-Boltzmann method is different from conventional finite difference, finite volume, or finite element methods in that it does not solve the Navier-Stokes equations directly. Rather, it simulates the evolution of a simplified fluid molecular velocity distribution on a rectangular, space-filling lattice. The propagation and relaxation of this molecular velocity distribution are designed such that fluid density, momentum, and stresses, being the zeroth, first and second order moments of the velocity distribution, obey the Navier-Stokes equations on large length and time scales. Our lattice-Boltzmann method employs a 19-velocity model (commonly referred to as D3Q19 model to denote that the simulations are in three dimensions and that the continuous distribution of the fluid molecular velocity is discretized as a sum of 19 discrete velocity quadratures) in which the density of the fluid  $\rho_g = 36$ . The viscosity of the fluid, which controls the relaxation rate of the non-equilibrium molecular velocity distribution, was set to  $\mu = 6.0$ , a good choice for low-Reynolds-number flows. The size of the smaller spheres was chosen to be  $9.6 \Delta x$  where  $\Delta x$  is the lattice spacing. In our previous study,<sup>18</sup> we conducted grid resolution tests and found that there is no significant difference between results obtained with  $d = 9.6 \Delta x$  and those with  $d = 12.5 \Delta x$ . Therefore,  $9.6 \Delta x$  was used to resolve the smaller spheres throughout this study.

In bidisperse gas–solid suspensions, because of the relative motion between particle species, lubrication interactions

between particles are very important. In our lattice-Boltzmann method, the lubrication interactions between spheres are solved analytically and imposed to the lattice solutions in an explicit manner. The detail of the implementation can be found in the paper by Nguyen and Ladd.<sup>42</sup> It was shown that when the particles are separated by more than one lattice spacing, the lattice-Boltzmann method can fully resolve the hydrodynamic interaction between the particles; when the distance between particles is less than one lattice spacing, the lubrication forces obtained from the lattice-Boltzmann no longer increase with decreasing separation, and corrections are applied to normal and tangential forces and torques so that they agree with the analytical solutions.<sup>43</sup>

The lubrication forces between two spheres with different velocities diverge as the separation between the spheres approaches zero. In reality, this divergence may be removed by surface roughness, finite weight of particles, or noncontinuum effects. All of these effects may be approximated in our simulations by specifying a cutoff distance  $\lambda$ : when the separation between particles becomes less than  $\lambda$ , the lubrication forces no longer increase but remain as constants. Our previous study<sup>18</sup> revealed that the particle-particle drag transmitted through the fluid increases with decreasing  $\lambda$  following a logarithmic scale, indicating that the lubrication forces in the normal direction is the primary contribution to the hydrodynamic particle-particle drag. In this study, we will also vary the values of  $\lambda$  to study the dependence of the drag forces on the lubrication cutoff distance.

We began our simulations by first randomly distributing spherical particles of different sizes in cubic, periodic domains, the size of which is typically 12–20 times the diameter of the smaller particles. Then, we employed Monte-Carlo steps to move the spheres in a random manner such that that all of our simulations began with the well-known microstructure of a binary hard-sphere fluid. This step is important because the drag forces would vary with the microstructure of the suspension. As there is no general knowledge on the microstructure of bidisperse gas-solid suspension, assuming all particles are intimately mixed and using a microstructure identical to that of a binary hard-sphere fluid provide a reasonable starting point. In Figure 1, we compared the structure factors of our initial particle configurations with the analytical solutions for a binary hard sphere fluid of the same composition.<sup>44</sup> The structure factors  $S_{11}(k)$ ,  $S_{22}(k)$ , and  $S_{12}(k)$  are measures of the microstructure of a bidisperse suspension, and are defined as the sums of particle relative positions in the Fourier space:

$$\begin{aligned} S_{11}(\mathbf{k}) &= \frac{1}{N_1} \left\langle \sum_{1-1\text{pairs}} e^{-i\mathbf{k}\cdot\mathbf{r}_{ij}} \right\rangle \\ S_{22}(\mathbf{k}) &= \frac{1}{N_2} \left\langle \sum_{2-2\text{pairs}} e^{-i\mathbf{k}\cdot\mathbf{r}_{ij}} \right\rangle \\ S_{12}(\mathbf{k}) &= \frac{1}{\sqrt{N_1 N_2}} \left\langle \sum_{1-2\text{pairs}} e^{-i\mathbf{k}\cdot\mathbf{r}_{ij}} \right\rangle. \end{aligned} \quad (20)$$

In Eq. 20,  $\mathbf{k}$  is the wave number vector, and  $\mathbf{r}_{ij}$  is the separation vector between a pair of particles. Unlike in previous discussions where  $i$  and  $j$  were used to index particle species, here  $i$  and  $j$  are indices to *individual* particles.  $S_{11}$  and  $S_{22}$

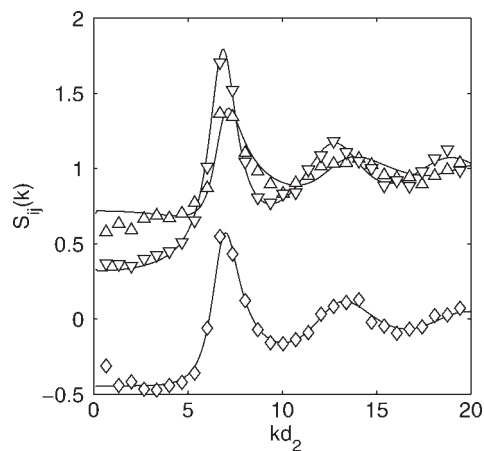


**Figure 1. Structure factors  $S_{11}(k)$  (upper triangles),  $S_{22}(k)$  (downward triangles), and  $S_{12}(k)$  (diamonds) calculated from 260 random configurations.**

The particle sizes are:  $d_1 = 9.6\Delta x$ ,  $d_2 = 10.66\Delta x$ ; there are 301 particles of type 1 and 449 particles of type 2; the volume fractions are:  $\phi_1 = 0.139$ ,  $\phi_2 = 0.285$ . The solid lines are based on the analytical solutions for  $S_{11}$ ,  $S_{22}$ , and  $S_{12}$  in Ashcroft and Langreth.<sup>44</sup>

were calculated by summing  $r_{ij}$  over pairs consisting of identical particles, i.e., 1-1 pairs and 2-2 pairs;  $S_{12}$ , on the other hand, was calculated by summing  $r_{ij}$  over 1-2 pairs. These structure factors are functions of particle sizes, volume fractions, and the magnitude of the wave number vector  $k = |\mathbf{k}|$  due to the isotropy of our suspensions. In Figure 1, the particle size ratio  $d_1:d_2$  was 1:1.11, the volume fractions were  $\phi_1 = 0.139$  and  $\phi_2 = 0.285$ . It may be observed that the structure factors calculated from ensemble averages of 260 configurations (750 particles in each configuration) agree very well with the analytical solutions provided by Ashcroft and Langreth.<sup>44</sup>

After obtaining initial particle configurations, we assigned a uniform velocity  $U$  to all particles if the configurations were for fixed-bed simulations, or velocities  $U_1$  and  $U_2$  to different particle species if they were for bidisperse suspension simulations with particle-particle relative motion. In both cases, the assigned velocities would generate a fluid flow within the particle assembly; meanwhile, a pressure gradient was applied to the fluid to ensure that the average fluid velocity  $U_g$  is zero. The velocities assigned to the particles thus became equivalent to the relative velocities to the fluid. Once the flow reached the steady state, the net fluid-particle interactive forces  $F_1$  and  $F_2$  acting on the particles were obtained by integrating the hydrodynamic stresses over particle surfaces and averaging over all particles of the same species. The drag forces  $F_{D1}$  and  $F_{D2}$  were then calculated from

$$F_{Di} = F_i + \frac{\pi d_i^3}{6} \frac{dP}{dx}, \quad (21)$$

where  $dP/dx$  is the bulk pressure gradient acting on the fluid that balances the total forces

$$-\frac{dP}{dx} = n_1 F_1 + n_2 F_2. \quad (22)$$

**Table 1. List of Bidisperse Fixed-Bed Simulations Conducted**

| Size Ratio        | $N_1/N_2$    | $\phi_1/\phi_2/M$ | $F_{D1\text{-fixed}}^*$ | $F_{D2\text{-fixed}}^*$ |
|-------------------|--------------|-------------------|-------------------------|-------------------------|
| $d_1:d_2 = 1:1.5$ | 345/409      | 0.02/0.08/10      | $2.09 \pm 0.01$         | $2.64 \pm 0.01$         |
|                   | 863/256      | 0.05/0.05/10      | $2.34 \pm 0.01$         | $3.08 \pm 0.04$         |
|                   | 1382/102     | 0.08/0.02/10      | $2.23 \pm 0.01$         | $2.90 \pm 0.03$         |
|                   | 863/512      | 0.05/0.10/10      | $2.77 \pm 0.01$         | $3.69 \pm 0.03$         |
|                   | 1209/409     | 0.07/0.08/10      | $2.86 \pm 0.01$         | $3.83 \pm 0.02$         |
|                   | 1382/358     | 0.08/0.07/10      | $2.91 \pm 0.01$         | $3.94 \pm 0.02$         |
|                   | 1727/256     | 0.10/0.05/10      | $3.01 \pm 0.01$         | $4.11 \pm 0.02$         |
|                   | 863/768      | 0.05/0.15/10      | $3.43 \pm 0.01$         | $4.71 \pm 0.03$         |
|                   | 728/216      | 0.10/0.10/9       | $3.68 \pm 0.01$         | $5.20 \pm 0.03$         |
|                   | 863/1023     | 0.05/0.20/10      | $4.21 \pm 0.01$         | $6.02 \pm 0.03$         |
|                   | 1093/216     | 0.15/0.10/10      | $4.82 \pm 0.02$         | $7.02 \pm 0.07$         |
|                   | 728/432      | 0.10/0.20/10      | $5.56 \pm 0.02$         | $8.23 \pm 0.06$         |
|                   | 1457/216     | 0.20/0.10/10      | $6.24 \pm 0.03$         | $9.45 \pm 0.06$         |
|                   | 364/648      | 0.05/0.30/12      | $6.53 \pm 0.05$         | $9.83 \pm 0.05$         |
|                   | 728/648      | 0.10/0.30/10      | $8.70 \pm 0.04$         | $13.60 \pm 0.09$        |
|                   | 1457/432     | 0.20/0.20/10      | $9.55 \pm 0.02$         | $15.23 \pm 0.10$        |
| 2186/216          | 0.30/0.10/10 | $10.45 \pm 0.03$  | $17.02 \pm 0.14$        |                         |
| $d_1:d_2 = 1:2.5$ | 728/47       | 0.10/0.10/4       | $3.31 \pm 0.01$         | $7.57 \pm 0.56$         |
|                   | 728/93       | 0.10/0.20/4       | $4.61 \pm 0.09$         | $11.29 \pm 0.42$        |
|                   | 1457/47      | 0.20/0.10/5       | $5.82 \pm 0.02$         | $15.75 \pm 0.38$        |
|                   | 728/140      | 0.10/0.30/5       | $6.71 \pm 0.03$         | $17.78 \pm 0.70$        |
|                   | 1457/93      | 0.20/0.20/4       | $8.18 \pm 0.03$         | $23.70 \pm 0.45$        |
|                   | 2186/47      | 0.30/0.10/5       | $9.84 \pm 0.06$         | $31.17 \pm 1.55$        |
| $d_1:d_2 = 1:4$   | 863/27       | 0.05/0.10/14      | $2.26 \pm 0.01$         | $6.64 \pm 0.24$         |
|                   | 863/40       | 0.05/0.15/20      | $2.57 \pm 0.01$         | $7.63 \pm 0.20$         |
|                   | 1727/27      | 0.10/0.10/15      | $3.14 \pm 0.01$         | $11.41 \pm 0.37$        |
|                   | 863/54       | 0.05/0.20/20      | $2.98 \pm 0.01$         | $9.76 \pm 0.26$         |
|                   | 2590/27      | 0.15/0.10/16      | $4.19 \pm 0.01$         | $18.18 \pm 0.45$        |
|                   | 1727/54      | 0.10/0.20/14      | $4.15 \pm 0.02$         | $16.45 \pm 0.38$        |
|                   | 3454/27      | 0.20/0.10/15      | $5.51 \pm 0.01$         | $27.67 \pm 1.42$        |
|                   | 863/81       | 0.05/0.30/9       | $4.04 \pm 0.03$         | $14.66 \pm 0.62$        |
|                   | 4317/27      | 0.25/0.10/8       | $7.20 \pm 0.01$         | $41.19 \pm 1.74$        |
|                   | 1727/81      | 0.10/0.30/13      | $5.72 \pm 0.02$         | $25.34 \pm 0.83$        |
|                   | 3454/54      | 0.20/0.20/9       | $7.52 \pm 0.02$         | $40.38 \pm 2.04$        |
|                   | 5180/27      | 0.30/0.10/10      | $9.42 \pm 0.01$         | $59.34 \pm 3.12$        |

The first column contains the numbers of particles in fixed beds; the second column contains the volume fractions and the number of configurations; the last two columns contain the normalized drag forces as defined in Eq. 10.

Note that all particles were frozen on the lattice, i.e., the positions of particles were not updated based on their velocities. This procedure is valid because of the quasi-steadiness of low-Re flows, and it ensures that the microstructure of the suspension remains unchanged in the course of a simulation.

We also exploited the linear characteristics of low-Re flows to characterize the friction coefficients for fixed beds and suspensions. For fixed beds, the friction coefficients  $\beta_i$  were obtained as  $f_{Di\text{-fixed}}/\Delta U$ ; for suspensions, we first let  $U_2 = 0$  and  $U_1$  be a non-zero value and solve for the 11 and 21 components of  $B_{ij}^*$  and  $\beta_{ij}^*$ , then we ran another set of simulations with  $U_1 = 0$  and non-zero  $U_2$  to characterize the 12 and 22 components.

### Drag in Polydisperse Fixed Beds

We now revisit the fluid-particle drag in bidisperse fixed beds. Because this problem has already been studied by van der Hoef et al.<sup>8,9</sup> it is an excellent opportunity for comparison and validation. In addition, an accurate drag law for bidisperse fixed beds is critically important for the development of a general drag law for bidisperse suspensions with particle-particle relative motion, because the general drag law must be able to recover the drag law for fixed beds when particle-particle relative motion is absent.

In order to characterize fluid-particle drag forces in bidisperse fixed beds, we conducted 361 simulations for 35 different combinations of  $(\phi_1, \phi_2, d_1/d_2)$ , listed in Table 1. The drag formula Eq. 12 developed by van der Hoef et al.<sup>8,9</sup> is good for bidisperse fixed beds with moderately different particle sizes (within a relatively narrow range of  $y_i$  in the vicinity of  $y_i = 1$ ), and the agreement between Eq. 12 and the numerical data with large particle size ratios (1:4 in particular) was rather poor. For this reason, in our simulations we emphasized more on fixed beds with large particle size ratios and extended the range of  $y_i$  considerably. In Figure 2 where we plotted  $F_{Di\text{-fixed}}^*/F_{D\text{-fixed}}^*$  ( $F_{D\text{-fixed}}^*$  given by Eq. 7) as a function of  $y_i$ , an excellent agreement between our data and those by van der Hoef et al.<sup>8,9</sup> is observed over the range of  $y_i$  where the two data sets overlap. The extended range of  $y_i$  in our data sets confirmed that the simple linear relation  $F_{Di\text{-fixed}}^*/F_{D\text{-fixed}}^* = y_i$  is only accurate in the vicinity of  $y_i = 1$  and becomes rather poor when  $y_i$  becomes much larger than unity. Besides, Eq. 12 predicts  $F_{Di\text{-fixed}}^* = 0$  when  $y_i \rightarrow 0$ , which does not agree with the general trend of the data in the low  $y_i$  limit. Even though the formula with  $O(y_i^3)$  terms [Eq. 14] improved the quality of fitting for large  $y_i$ , the discrepancy in the low  $y_i$  limit is not addressed. Moreover, the additional dependence of  $F_{Di\text{-fixed}}^*/F_{D\text{-fixed}}^*$  on the particle size ratio, in view of Figure 2,

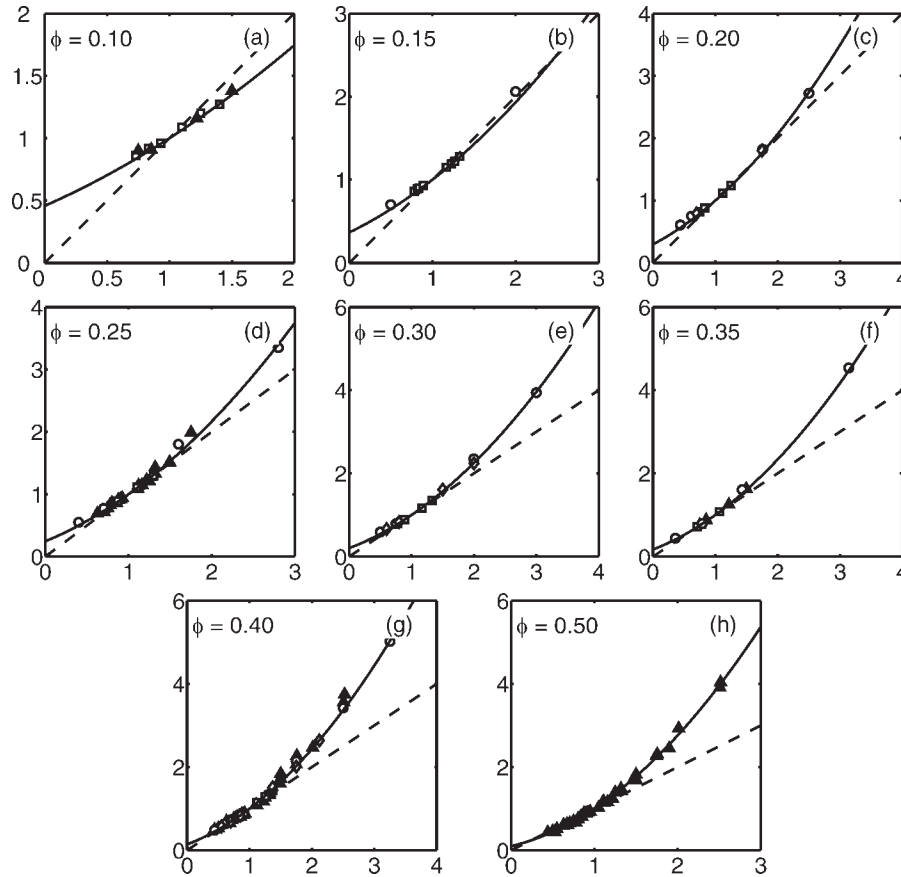


**Figure 2.** The vertical axis is the dimensionless drag in bidisperse fixed beds normalized by the dimensionless drag in monodisperse fixed beds of the same volume fraction  $F_{Di\text{-fixed}}^*/F_{D\text{-fixed}}^*$ ; the horizontal axis is the dimensionless particle size ratio  $y_i = d_i/\langle d \rangle$ .  $F_{D\text{-fixed}}^*$  was calculated based on Eq. 7.

This figure shows that (1) our simulation data, represented by the squares ( $d_1:d_2 = 1:1.5$ ), diamonds ( $d_1:d_2 = 1:2.5$ ), and circles ( $d_1:d_2 = 1:4$ ), are in very good agreement with the data by van der Hoef et al.<sup>8,9</sup> (solid triangles), and (2)  $F_{Di\text{-fixed}}^*/F_{D\text{-fixed}}^*$  is only a function of  $\phi$  and  $y_i$ . The dashed lines are based on van der Hoef et al.'s drag law Eq. 12<sup>8,9</sup>; the solid lines are based on our new drag law for bidisperse fixed beds Eqs. 23 and 25.

does not appear to be very necessary. Hence, we will assume that  $F_{Di\text{-fixed}}^*/F_{D\text{-fixed}}^*$  can still be fit by a simple function of  $\phi$  and  $y_i$ , and, in order to account for the nonlinear dependence of  $F_{Di\text{-fixed}}^*/F_{D\text{-fixed}}^*$  on  $y_i$ , we will develop a quadratic function to fit the numerical data.

In view of the limitations of Eqs. 12 and 14 and the limiting behaviors of  $F_{Di\text{-fixed}}^*$ , we propose three conditions that  $F_{Di\text{-fixed}}^*$  must satisfy to guide the design of the quadratic fitting function, and these conditions are listed below.

- $F_{Di\text{-fixed}}^*/F_{D\text{-fixed}}^* = 1$  when  $y_i = 1$ . This condition is needed such that the new drag law can reproduce the drag of a monodisperse fixed suspension when all  $d_i$  equal. While Eq. 12 satisfies this condition, Eq. 14 does not.

- $F_{Di\text{-fixed}}^* \rightarrow 1$  when  $\phi \rightarrow 0$ . This condition is needed because in the dilute limit every particle will be subjected to its respective Stokes drag, and it agrees with the trend observed in Figure 2. Neither Eq. 12 nor Eq. 14 satisfies this condition.

- $F_{Di\text{-fixed}}^* \rightarrow 1/(1 - \phi)$  when  $y_i \rightarrow 0$ . In a bidisperse suspension, the scaled particle size  $y_1$  would approach zero when  $d_1 \ll d_2$  and  $\phi_1 \ll \phi_2$ . In this limit, because the average distance between smaller particles and larger particles and that between smaller particles themselves are

much larger than  $d_1$ , the smaller particles can be treated as point particles and the fluid-particle drag force acting on a smaller particle is simply the Stokes drag based on the local fluid velocity. The average drag force  $F_{D1\text{-fixed}}$  is therefore the Stokes drag based on the average fluid velocity relative to the particle assembly  $3\pi\mu d_1 \Delta U$ , and  $F_{D1\text{-fixed}}^* = 1/(1 - \phi)$ .

The simplest quadratic fitting function that satisfies the above conditions is

$$F_{Di\text{-fixed}}^* = \frac{1}{1 - \phi} + \left( F_{D\text{-fixed}}^* - \frac{1}{1 - \phi} \right) [ay_i + (1 - a)y_i^2], \quad (23)$$

where  $a$  can be obtained from linear regression

$$\frac{F_{Di\text{-fixed}}^* - \frac{1}{1 - \phi}}{F_{D\text{-fixed}}^* - \frac{1}{1 - \phi}} - y_i^2 = a(y_i - y_i^2). \quad (24)$$

Figure 3 shows that  $(F_{Di\text{-fixed}}^* - \frac{1}{1 - \phi}) / (F_{D\text{-fixed}}^* - \frac{1}{1 - \phi}) - y_i^2$  can be very well approximated by linear functions of  $y_i - y_i^2$ . As indicated by Figure 4, the values of  $a$  generally decrease with increasing volume fraction, and can be fit by a third-order polynomial

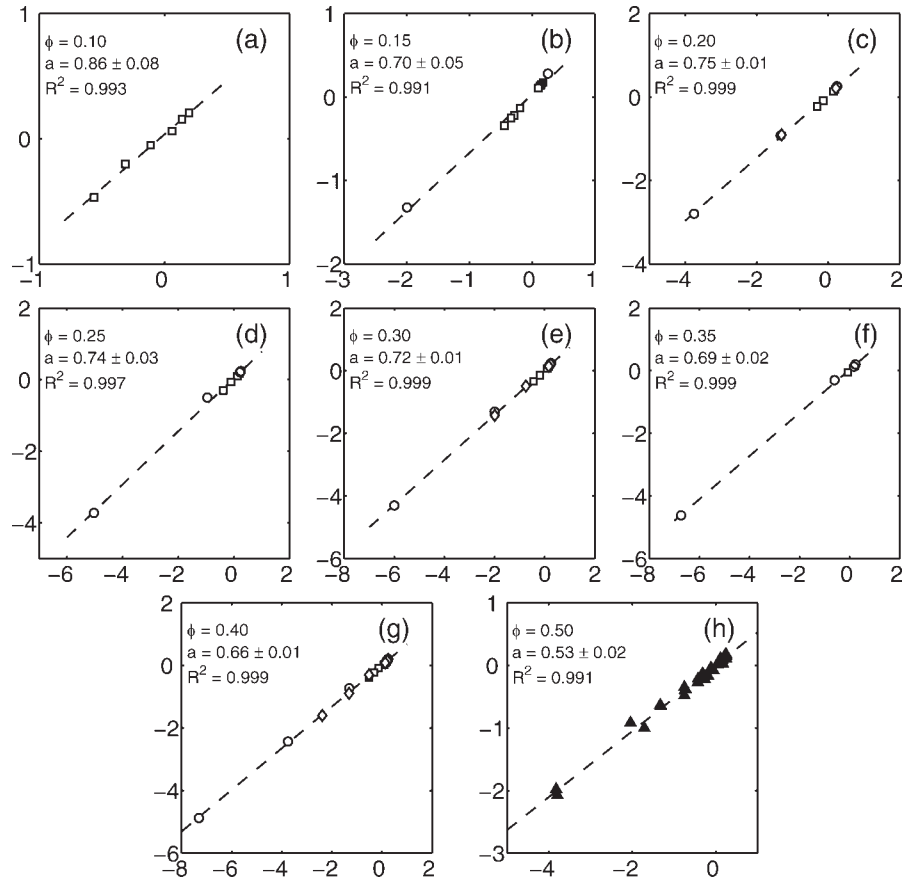


**Figure 3.** This figure shows the linear relation between  $(F_{Di\text{-fixed}}^* - \frac{1}{1-\phi}) / (F_{D\text{-fixed}}^* - \frac{1}{1-\phi}) - y_i^2$ , the vertical axis, and  $y_i - y_i^2$ , the horizontal axis.

According to Eq. 24, the slopes of the best linear fits yield the values of  $a(\phi)$ , the fitting function in the new drag law for bidisperse fixed beds Eq. 23. In graphs (a) through (h), the symbols are the simulation data and the dashed lines are the best linear fits. The slopes of the lines and the  $R^2$  values are included in the figure. The meanings of the symbols are identical to those in Figure (2).

$$a(\phi) = 1 - 2.660\phi + 9.096\phi^2 - 11.338\phi^3. \quad (25)$$

In Figure 2, the predictions based on Eqs. 23 and 25 were included as solid lines. Compared with the predictions based on Eq. 12 (dotted lines), the solid lines are clearly better in the volume fraction range of  $0.1 < \phi < 0.5$ . The average deviation of this new drag law from the simulation data, defined as the square root of the mean square percentage deviations, is only 3.9%; the maximum deviation is 9.4%.

Equations 23 and 25 can be readily applied to polydisperse fixed beds with three or more sizes of particles. For general polydisperse suspensions and fixed beds, the Sauter mean  $\langle d \rangle$  is defined as

$$\langle d \rangle = \frac{\sum_i (n_i d_i^3)}{\sum_i (n_i d_i^2)} \quad (26)$$

We simulated a low-Re flow through a ternary fixed bed with  $d_1 = 9.6 \Delta x$ ,  $d_2 = 12 \Delta x$ , and  $d_3 = 14.4 \Delta x$ . The volume fractions are  $\phi_1 = \phi_2 = \phi_3 = 0.07$ . The size of the cubic computational domain is 15.6 times the size of the smallest particles ( $150 \Delta x$ ). On the basis of these parameters, it is easy

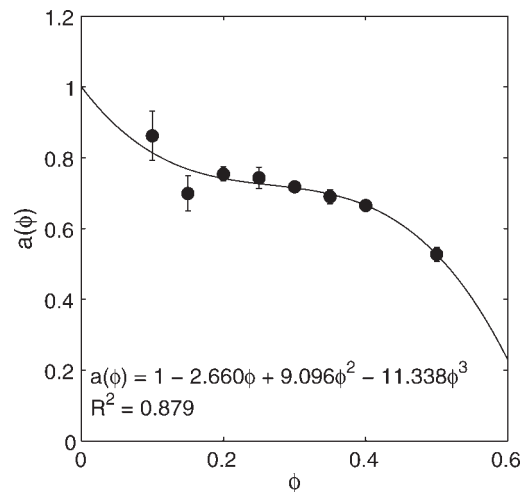


**Figure 4.** The slopes obtained in Fig. 3 are plotted here as a function of  $\phi$ .

These data points can be fit by a third-order polynomial, which is Eq. 25. The error bars represent 95% confidence intervals of the linear fitting.

to obtain  $y_1 = 0.822$ ,  $y_2 = 1.028$ , and  $y_3 = 1.233$ . Substituting  $y_i$  and  $\phi_i$  into Eqs. 23 and 25, we obtained  $F_{D1\text{-fixed}}^* = 3.94$ ,  $F_{D2\text{-fixed}}^* = 4.64$ , and  $F_{D3\text{-fixed}}^* = 5.45$ ;  $F_{Di\text{-fixed}}^*$  found from simulations (averaged over 10 runs with different particle configurations) are 3.74, 4.53, and 5.39 respectively for the three particle species, in good agreement with the predictions.

Even though Eq. 23 was developed to facilitate the development of a drag law for suspensions with particle-particle relative motions, an accurate drag law for polydisperse fixed beds has its own merits and can be useful for many practical applications. In addition, dense polydisperse fixed beds can be regarded as porous media with grain size distributions, and an expression for the overall permeability would be very informative for researchers and engineers interested in porous media flows. With this in mind, we invoke Eq. 13 and rewrite Eq. 23 into

$$\beta_i = \frac{18\phi_i(1-\phi)\mu}{d_i^2} \left[ \frac{1}{1-\phi} + (F_{D\text{-fixed}}^* - \frac{1}{1-\phi}) [ay_i + (1-a)y_i^2] \right], \quad (27)$$

The total drag force per unit volume is therefore

$$\begin{aligned} \sum_i f_{Di\text{-fixed}} &= -18(1-\phi)\mu\Delta U \sum_i \frac{\phi_i}{d_i^2} \\ &\times \left[ \frac{1}{1-\phi} + (F_{D\text{-fixed}}^* - \frac{1}{1-\phi}) [ay_i + (1-a)y_i^2] \right] \\ &= -\frac{18\phi(1-\phi)\mu\Delta U}{\langle d \rangle^2} \\ &\times \left[ F_{D\text{-fixed}}^* + \frac{\langle d \rangle^2}{2\phi^2(1-\phi)} \sum_i \sum_j \phi_i \phi_j \left( \frac{1}{d_i} - \frac{1}{d_j} \right)^2 \right] \end{aligned} \quad (28)$$

It is interesting to note that  $a(\phi)$  disappeared in the summation. Since the total drag force is related to the pressure gradient by

$$\sum_i f_{Di\text{-fixed}} = (1-\phi) \frac{dP}{dx}, \quad (29)$$

one can obtain the relation between  $dP/dx$  and the superficial velocity  $U_s = (1-\phi)\Delta U$  of the fluid through the porous medium

$$\begin{aligned} \frac{dP}{dx} &= -\frac{18\phi\mu U_s}{(1-\phi)\langle d \rangle^2} \\ &\times \left[ F_{D\text{-fixed}}^* + \frac{\langle d \rangle^2}{2\phi^2(1-\phi)} \sum_i \sum_j \phi_i \phi_j \left( \frac{1}{d_i} - \frac{1}{d_j} \right)^2 \right]. \end{aligned} \quad (30)$$

Compared with the corresponding relation for a porous medium formed by monodisperse spheres

$$\frac{dP}{dx} = -\frac{18\phi\mu U_s}{(1-\phi)d^2} F_{D\text{-fixed}}^*, \quad (31)$$

Equation 30 clearly indicates that the permeability of a porous medium with grain size distribution is always lower than the permeability of a porous medium consisting of mono-

disperse spheres of the same volume fraction under the condition  $d = \langle d \rangle$ . For dense bidisperse fixed beds, it is straightforward to show that the change in the permeability due to bidispersity is usually small, and it is safe to neglect the  $\phi_1 \phi_2$  term in Eq. 30. However, at low volume fractions the difference becomes much more significant. As our fixed-bed drag law also serves as a stepping-stone for the subsequent development of the general drag law for fluidized bidisperse gas-solid suspensions with particle-particle relative motions, the accuracy in the dilute regime is also of critical importance to us.

Note that van der Hoef et al.<sup>8,9</sup> provided a seemingly opposite statement that the total drag force of a polydisperse fixed bed is lower than a monodisperse fixed bed of the same volume fraction, giving rise to a higher permeability. To understand this difference, it is important to realize that the comparison in van der Hoef et al.<sup>8,9</sup> is different and is between a polydisperse fixed bed and a monodisperse fixed bed with particle size  $\bar{d}$  rather than  $\langle d \rangle$ .  $\bar{d}$ , being the number average of all particle sizes in the polydisperse fixed bed, is always smaller than the Sauter mean  $\langle d \rangle$ . Our drag law Eq. 30 is consistent with van der Hoef et al.<sup>8,9</sup> if we neglect the  $\phi_i \phi_j$  terms and compare to a monodisperse fixed bed containing particles of size  $\bar{d}$  rather than  $\langle d \rangle$ .

To develop a formula capable of handling a continuous size distribution, let  $\sigma_i = n_i / (\sum_i n_i)$  be the fraction of the  $i$ th particle species and it is easy to obtain

$$\phi_i = \frac{\pi \sigma_i d_i^3}{6} \left( \sum_i n_i \right). \quad (32)$$

Because the sum of all  $\phi_i$  yields  $\phi$ , the total solid fraction of a porous medium, a relation between  $(\sum_i n_i)$ , the total number of particles per unit volume, and  $\phi$  can be established

$$\phi = \frac{\pi}{6} \left( \sum_i \sigma_i d_i^3 \right) \left( \sum_i n_i \right). \quad (33)$$

By substituting Eq. 33 into Eq. 32, we can write  $\phi_i$  in terms of  $\phi$  and  $\sigma_i$

$$\phi_i = \phi \frac{\sigma_i d_i^3}{\sum_i \sigma_i d_i^3}. \quad (34)$$

Substituting Eq. 34 into Eq. 30, and using  $\langle d \rangle = (\sum_i \sigma_i d_i^3) / (\sum_i \sigma_i d_i^2)$ , we obtain

$$\frac{dP}{dx} = -\frac{18\phi\mu U_s}{(1-\phi)\langle d \rangle^2} \left[ F_{D\text{-fixed}}^* + \frac{\sum_i \sum_j \sigma_i \sigma_j d_i d_j (d_i - d_j)^2}{2(1-\phi)(\sum_i \sigma_i d_i^2)^2} \right]. \quad (35)$$

Equation 35 can be further simplified to

$$\begin{aligned} \frac{dP}{dx} &= -\frac{18\phi\mu U_s}{(1-\phi)\langle d \rangle^2} \\ &\times \left[ F_{D\text{-fixed}}^* + \frac{1}{1-\phi} \left[ \frac{(\sum_i \sigma_i d_i)(\sum_i \sigma_i d_i^3)}{(\sum_i \sigma_i d_i^2)^2} - 1 \right] \right]. \end{aligned} \quad (36)$$

Now, assume that the porous medium of interest is formed by grains whose size is described by a continuous size distribution  $\sigma(d)$ , let  $\sigma_I$ ,  $\sigma_{II}$ , and  $\sigma_{III}$  denote the first, second, and third order moments of  $\sigma(d)$ , Eq. 36 indicates that the relation between the pressure gradient and superficial velocity of the fluid flowing through this porous medium is simply

$$\frac{dP}{dx} = -\frac{18\phi\mu U_s}{(1-\phi)\langle d \rangle^2} \left[ F_{D\text{-fixed}}^* + \frac{1}{1-\phi} \left( \frac{\sigma_I\sigma_{III}}{\sigma_{II}^2} - 1 \right) \right]. \quad (37)$$

Let us substitute two common particle size distributions—Gaussian and log-normal distributions—into Eq. 37 and examine the influence of the size distribution on the overall drag. If the size distribution is Gaussian

$$\sigma(d) = \frac{1}{\delta\sqrt{2\pi}} \exp\left(-\frac{(d-\bar{d})^2}{2\delta^2}\right), \quad (38)$$

then  $\sigma_I = \bar{d}$ ,  $\sigma_{II} = \bar{d}^2 + \delta^2$ , and  $\sigma_{III} = \bar{d}^3 + 3\delta^2\bar{d}$ . It is easy to show that Eq. 37 becomes

$$\frac{dP}{dx} = -\frac{18\phi\mu U_s}{(1-\phi)\langle d \rangle^2} \left[ F_{D\text{-fixed}}^* + \frac{1}{1-\phi} \frac{(\bar{d}/\delta)^2 - 1}{(\bar{d}/\delta)^4 + 2(\bar{d}/\delta)^2 + 1} \right]. \quad (39)$$

On the other hand, if the size distribution is log-normal

$$\sigma(d) = \frac{1}{d\delta^*\sqrt{2\pi}} \exp\left(-\frac{(\ln d - \ln \bar{d})^2}{2\delta^{*2}}\right), \quad (40)$$

then  $\sigma_I = \bar{d}e^{\delta^{*2}/2}$ ,  $\sigma_{II} = \bar{d}^2e^{2\delta^{*2}}$ ,  $\sigma_{III} = \bar{d}^3e^{9\delta^{*2}/2}$ , and Eq. 37 becomes

$$\frac{dP}{dx} = -\frac{18\phi\mu U_s}{(1-\phi)\langle d \rangle^2} \left[ F_{D\text{-fixed}}^* + \frac{1}{1-\phi} (e^{\delta^{*2}} - 1) \right]. \quad (41)$$

Note that  $\delta$  in Eq. 38 and  $\delta^*$  in Eq. 40 have different meanings and units. In Eq. 38,  $\delta$  represents the standard deviation of the distribution and has the unit of length; in Eq. 40,  $\delta^*$  yields the shape of the distribution and is dimensionless and typically less than unity. When  $\delta^*$  becomes less than about 0.25, the shape of the log-normal distribution becomes approximately Gaussian.

With these equations, we can now answer a practical question: how good the approximation would be if we neglect the second correction term on the right hand side of Eq. 37 and assume that the drag of a polydisperse fixed bed (or a porous medium with grain size distribution) equals the drag of a monodisperse fixed bed with  $d = \langle d \rangle$ ? In Figure 5, we plotted  $\sigma_I\sigma_{III}/\sigma_{II}^2 - 1$  as a function of  $\bar{d}/\delta$  for Gaussian distributions and as a function of  $\delta^*$  for log-normal distributions. For Gaussian distributions, the value of  $\sigma_I\sigma_{III}/\sigma_{II}^2 - 1$  for all practical  $\bar{d}/\delta$  never exceeds 0.13. Compared with the values of  $F_{D\text{-fixed}}^*(1-\phi)$  which are typically 1–10 when  $\phi < 0.5$ ,  $\sigma_I\sigma_{III}/\sigma_{II}^2 - 1$  is indeed a small correction and can be neglected under most occasions. For log-normal distributions, however,  $\sigma_I\sigma_{III}/\sigma_{II}^2 - 1$  can become comparable to  $F_{D\text{-fixed}}^*(1-\phi)$  when  $\delta^*$  becomes close to unity. When this happens, neglecting  $\sigma_I\sigma_{III}/\sigma_{II}^2 - 1$  term would introduce rather significant errors and should not be practiced.

### Drag in Polydisperse Gas–Solid Suspensions with Particle–Particle Relative Motion

We now consider the fluid-particle drag in suspensions where the two particle species have different velocities relative to the fluid, i.e.  $\Delta U_1 \neq \Delta U_2$ . In this case, the fluid-particle drag will contain a particle–particle drag term that represents the momentum transfer between particle species due to hydrodynamic interactions. In a preceding numerical study, Yin and Sundaresan<sup>18</sup> characterized the special case where the two particle species are of the same size, i.e.,  $d_1 = d_2$ . In this study, we are interested in the more general situation of  $d_1 \neq d_2$ . We will show that the particle–particle drag due to hydrodynamic

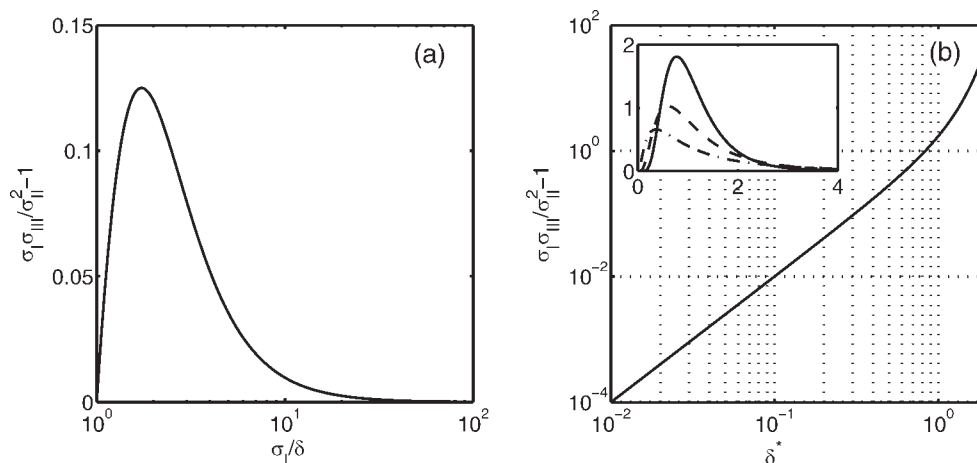


**Figure 5.**  $\sigma_I\sigma_{III}/\sigma_{II}^2 - 1$  as a function of  $\bar{d}/\delta$  for Gaussian particle size distributions (a), and as a function of  $\delta^*$  for log-normal particle size distributions (b).

The lines were calculated base on Eq. 39 and Eq. 41. The small insert in (b) shows the log-normal size distribution  $\sigma(d)\bar{d}$  as a function of  $d/\bar{d}$  for three values of  $\delta^*$ : 0.25 (solid line), 0.5 (dashed line), and 1.0 (dash-dot line).

**Table 2. List of Polydisperse Suspension Simulations with Particle–Particle Relative Motions**

| Size Ratio        | $\phi_1/\phi_2/M$ | $\beta_{11}^*$   | $\beta_{12}^*$    | $-\beta_{12}^*/\beta_{11}^*$ | $\beta_{21}^*$    | $\beta_{22}^*$   | $-\beta_{21}^*/\beta_{22}^*$ |      |
|-------------------|-------------------|------------------|-------------------|------------------------------|-------------------|------------------|------------------------------|------|
| $d_1:d_2 = 1:1.5$ | 0.05/0.05/15      | $2.89 \pm 0.04$  | $-0.26 \pm 0.04$  | 0.09                         | $-0.28 \pm 0.04$  | $1.77 \pm 0.04$  | 0.16                         |      |
|                   | 0.05/0.10/15      | $4.25 \pm 0.05$  | $-0.73 \pm 0.06$  | 0.17                         | $-0.75 \pm 0.05$  | $4.89 \pm 0.09$  | 0.15                         |      |
|                   | 0.10/0.05/15      | $6.30 \pm 0.04$  | $-0.58 \pm 0.05$  | 0.09                         | $-0.51 \pm 0.04$  | $2.35 \pm 0.05$  | 0.22                         |      |
|                   | 0.05/0.15/12      | $5.61 \pm 0.07$  | $-1.33 \pm 0.09$  | 0.24                         | $-1.23 \pm 0.07$  | $9.40 \pm 0.10$  | 0.13                         |      |
|                   | 0.10/0.10/14      | $9.11 \pm 0.15$  | $-1.47 \pm 0.13$  | 0.16                         | $-1.42 \pm 0.13$  | $6.25 \pm 0.14$  | 0.23                         |      |
|                   | 0.05/0.20/12      | $7.50 \pm 0.14$  | $-2.09 \pm 0.07$  | 0.28                         | $-2.18 \pm 0.13$  | $15.53 \pm 0.07$ | 0.14                         |      |
|                   | 0.15/0.10/15      | $15.49 \pm 0.16$ | $-2.42 \pm 0.15$  | 0.16                         | $-2.50 \pm 0.14$  | $8.04 \pm 0.15$  | 0.31                         |      |
|                   | 0.10/0.20/12      | $16.08 \pm 0.11$ | $-4.18 \pm 0.19$  | 0.26                         | $-4.48 \pm 0.11$  | $19.57 \pm 0.18$ | 0.23                         |      |
|                   | 0.20/0.10/15      | $23.81 \pm 0.21$ | $-3.66 \pm 0.24$  | 0.15                         | $-3.90 \pm 0.23$  | $10.40 \pm 0.23$ | 0.38                         |      |
|                   | 0.05/0.30/12      | $12.09 \pm 0.18$ | $-4.75 \pm 0.29$  | 0.39                         | $-4.57 \pm 0.19$  | $34.90 \pm 0.31$ | 0.13                         |      |
|                   | 0.10/0.30/12      | $28.44 \pm 0.56$ | $-10.90 \pm 0.59$ | 0.38                         | $-11.86 \pm 0.56$ | $45.74 \pm 0.58$ | 0.26                         |      |
|                   | 0.20/0.20/12      | $42.80 \pm 0.43$ | $-12.83 \pm 0.56$ | 0.30                         | $-13.10 \pm 0.48$ | $33.89 \pm 0.52$ | 0.38                         |      |
|                   | 0.30/0.10/12      | $48.93 \pm 0.31$ | $-9.10 \pm 0.31$  | 0.18                         | $-8.53 \pm 0.32$  | $18.86 \pm 0.32$ | 0.45                         |      |
|                   | $d_1:d_2 = 1:2.5$ | 0.10/0.10/13     | $11.31 \pm 0.21$  | $-1.53 \pm 0.22$             | 0.14              | $-1.54 \pm 0.22$ | $5.03 \pm 0.22$              | 0.31 |
|                   |                   | 0.10/0.20/12     | $20.06 \pm 0.43$  | $-4.61 \pm 0.41$             | 0.23              | $-3.91 \pm 0.47$ | $17.02 \pm 0.42$             | 0.23 |
| 0.20/0.10/15      |                   | $26.04 \pm 0.27$ | $-3.37 \pm 0.22$  | 0.13                         | $-3.21 \pm 0.24$  | $8.50 \pm 0.21$  | 0.38                         |      |
| 0.10/0.30/10      |                   | $37.27 \pm 0.83$ | $-12.30 \pm 0.87$ | 0.33                         | $-13.39 \pm 0.82$ | $43.12 \pm 0.89$ | 0.31                         |      |
| 0.20/0.20/12      |                   | $48.94 \pm 0.37$ | $-13.19 \pm 0.23$ | 0.27                         | $-12.87 \pm 0.41$ | $29.95 \pm 0.29$ | 0.43                         |      |
| 0.30/0.10/15      |                   | $51.78 \pm 0.45$ | $-7.69 \pm 0.44$  | 0.15                         | $-7.74 \pm 0.44$  | $15.16 \pm 0.43$ | 0.51                         |      |
| $d_1:d_2 = 1:4$   | 0.05/0.10/22      | $7.68 \pm 0.09$  | $-0.61 \pm 0.06$  | 0.08                         | $-0.72 \pm 0.09$  | $3.16 \pm 0.06$  | 0.23                         |      |
|                   | 0.05/0.15/20      | $11.15 \pm 0.15$ | $-1.78 \pm 0.16$  | 0.16                         | $-1.57 \pm 0.17$  | $7.06 \pm 0.14$  | 0.22                         |      |
|                   | 0.10/0.10/20      | $12.65 \pm 0.12$ | $-1.12 \pm 0.08$  | 0.09                         | $-1.03 \pm 0.08$  | $3.75 \pm 0.07$  | 0.27                         |      |
|                   | 0.05/0.20/20      | $15.18 \pm 0.26$ | $-2.65 \pm 0.31$  | 0.17                         | $-2.61 \pm 0.28$  | $12.79 \pm 0.31$ | 0.20                         |      |
|                   | 0.15/0.10/25      | $19.07 \pm 0.10$ | $-1.71 \pm 0.12$  | 0.09                         | $-1.74 \pm 0.10$  | $4.84 \pm 0.12$  | 0.36                         |      |
|                   | 0.10/0.20/14      | $25.66 \pm 0.27$ | $-4.16 \pm 0.21$  | 0.16                         | $-4.73 \pm 0.35$  | $14.54 \pm 0.23$ | 0.32                         |      |
|                   | 0.20/0.10/23      | $27.37 \pm 0.14$ | $-2.58 \pm 0.12$  | 0.09                         | $-2.66 \pm 0.14$  | $6.46 \pm 0.13$  | 0.41                         |      |
|                   | 0.05/0.30/12      | $25.03 \pm 0.65$ | $-6.14 \pm 0.69$  | 0.24                         | $-6.49 \pm 0.66$  | $31.56 \pm 0.76$ | 0.20                         |      |
|                   | 0.25/0.10/24      | $37.96 \pm 0.16$ | $-3.99 \pm 0.12$  | 0.10                         | $-3.84 \pm 0.16$  | $8.87 \pm 0.14$  | 0.43                         |      |
|                   | 0.10/0.30/14      | $43.77 \pm 0.73$ | $-11.62 \pm 0.88$ | 0.26                         | $-11.54 \pm 0.70$ | $38.50 \pm 0.88$ | 0.30                         |      |
|                   | 0.20/0.20/19      | $52.40 \pm 0.35$ | $-11.04 \pm 0.63$ | 0.21                         | $-10.70 \pm 0.34$ | $25.16 \pm 0.67$ | 0.42                         |      |
|                   | 0.30/0.10/21      | $52.36 \pm 0.19$ | $-6.60 \pm 0.19$  | 0.13                         | $-6.26 \pm 0.18$  | $12.79 \pm 0.20$ | 0.49                         |      |

The first column contains the volume fractions and the number of configurations; the second, third, fifth, and sixth columns contain the dimensionless volume-specific friction coefficient  $\beta_{ij}^*$ . The ratio of the off-diagonals to the diagonals in the fourth and last columns indicate the importance of the hydrodynamic particle–particle drag. In all simulations  $\lambda/d_1 = 0.01$ .

interaction is always an important part of the total fluid-particle drag, and present a drag formula for polydisperse gas–solid suspensions with particle–particle relative motion.

As discussed previously, the dimensionless fluid-particle drag forces per particle and per volume in bidisperse gas–solid suspensions can be expressed as linear functions of fluid-particle relative velocities [c.f. Eqs. 18 and 19]. From now on, we will focus on the volume specific drag law Eq. 19 and report the values of the volume specific friction coefficient  $\beta_{ij}^*$  for

different combinations of volume fractions, particle size ratios, and lubrication cutoff distances. The values for  $B_{ij}^*$  can be easily computed by invoking  $n_i B_{ij}^* \langle d \rangle^3 = \beta_{ij}^*$ .

In Table 2 through Table 5, we have listed all simulations conducted in this study with  $\Delta U_1 \neq \Delta U_2$ , including 504 simulations for the smallest lubrication cutoff  $\lambda/d_1 = 0.01$ , and 173 simulations for each of the higher lubrication cutoff values:  $\lambda/d_1 = 0.02, 0.05$ , and  $0.10$ . Also listed in these tables are the friction coefficients  $\beta_{ij}^*$  and the ratios  $-\beta_{12}^*/\beta_{11}^*$  and

**Table 3. List of Polydisperse Suspension Simulations with Particle–Particle Relative Motions**

| Size Ratio        | $\phi_1/\phi_2/M$ | $\beta_{11}^*$   | $\beta_{12}^*$    | $-\beta_{12}^*/\beta_{11}^*$ | $\beta_{21}^*$    | $\beta_{22}^*$   | $-\beta_{21}^*/\beta_{22}^*$ |
|-------------------|-------------------|------------------|-------------------|------------------------------|-------------------|------------------|------------------------------|
| $d_1:d_2 = 1:1.5$ | 0.10/0.10/14      | $8.88 \pm 0.11$  | $-1.21 \pm 0.09$  | 0.14                         | $-1.20 \pm 0.10$  | $5.99 \pm 0.10$  | 0.20                         |
|                   | 0.10/0.20/12      | $15.39 \pm 0.20$ | $-3.95 \pm 0.16$  | 0.26                         | $-3.67 \pm 0.23$  | $19.23 \pm 0.18$ | 0.19                         |
|                   | 0.20/0.10/15      | $23.24 \pm 0.16$ | $-3.09 \pm 0.18$  | 0.13                         | $-3.33 \pm 0.18$  | $9.83 \pm 0.18$  | 0.34                         |
|                   | 0.10/0.30/12      | $26.91 \pm 0.44$ | $-9.55 \pm 0.53$  | 0.35                         | $-10.33 \pm 0.43$ | $44.40 \pm 0.54$ | 0.24                         |
| $d_1:d_2 = 1:2.5$ | 0.10/0.10/12      | $11.12 \pm 0.18$ | $-1.26 \pm 0.20$  | 0.11                         | $-1.36 \pm 0.19$  | $4.77 \pm 0.20$  | 0.28                         |
|                   | 0.10/0.20/12      | $19.65 \pm 0.27$ | $-4.04 \pm 0.26$  | 0.20                         | $-3.50 \pm 0.31$  | $16.45 \pm 0.28$ | 0.21                         |
|                   | 0.20/0.10/15      | $25.75 \pm 0.20$ | $-2.96 \pm 0.16$  | 0.11                         | $-2.91 \pm 0.18$  | $8.10 \pm 0.15$  | 0.36s                        |
|                   | 0.10/0.30/10      | $35.66 \pm 0.55$ | $10.34 \pm 0.55$  | 0.29                         | $-11.54 \pm 0.57$ | $41.17 \pm 0.56$ | 0.28                         |
| $d_1:d_2 = 1:4$   | 0.10/0.10/20      | $12.52 \pm 0.07$ | $-0.94 \pm 0.04$  | 0.08                         | $-0.90 \pm 0.07$  | $3.57 \pm 0.05$  | 0.25                         |
|                   | 0.10/0.20/14      | $24.88 \pm 0.22$ | $-3.73 \pm 0.18$  | 0.15                         | $-3.95 \pm 0.24$  | $14.11 \pm 0.19$ | 0.28                         |
|                   | 0.20/0.10/24      | $27.02 \pm 0.10$ | $-2.26 \pm 0.08$  | 0.08                         | $-2.30 \pm 0.09$  | $6.14 \pm 0.10$  | 0.37                         |
|                   | 0.10/0.30/14      | $42.41 \pm 0.55$ | $-10.54 \pm 0.76$ | 0.25                         | $-10.18 \pm 0.52$ | $37.38 \pm 0.78$ | 0.27                         |

The first column contains the volume fractions and the number of configurations; the second, third, fifth, and sixth columns contain the dimensionless volume-specific friction coefficient  $\beta_{ij}^*$ . The ratio of the off-diagonals to the diagonals in the fourth and last columns indicate the importance of the hydrodynamic particle–particle drag. In all simulations  $\lambda/d_1 = 0.02$ .

**Table 4. List of Polydisperse Suspension Simulations with Particle–Particle Relative Motions**

| Size Ratio        | $\phi_1/\phi_2/M$ | $\beta_{11}^*$   | $\beta_{12}^*$   | $-\beta_{12}^*/\beta_{11}^*$ | $\beta_{21}^*$   | $\beta_{22}^*$   | $-\beta_{21}^*/\beta_{22}^*$ |
|-------------------|-------------------|------------------|------------------|------------------------------|------------------|------------------|------------------------------|
| $d_1:d_2 = 1:1.5$ | 0.10/0.10/14      | $8.61 \pm 0.08$  | $-0.94 \pm 0.06$ | 0.11                         | $-0.93 \pm 0.08$ | $5.72 \pm 0.07$  | 0.16                         |
|                   | 0.10/0.20/12      | $14.55 \pm 0.15$ | $-3.01 \pm 0.11$ | 0.21                         | $-2.83 \pm 0.18$ | $18.29 \pm 0.12$ | 0.15                         |
|                   | 0.20/0.10/15      | $22.46 \pm 0.09$ | $-2.41 \pm 0.12$ | 0.11                         | $-2.53 \pm 0.10$ | $9.15 \pm 0.12$  | 0.28                         |
|                   | 0.10/0.30/12      | $24.87 \pm 0.39$ | $-7.49 \pm 0.43$ | 0.30                         | $-8.29 \pm 0.36$ | $42.3 \pm 0.46$  | 0.20                         |
| $d_1:d_2 = 1:2.5$ | 0.10/0.10/13      | $10.87 \pm 0.13$ | $-1.11 \pm 0.15$ | 0.10                         | $-1.11 \pm 0.14$ | $4.62 \pm 0.14$  | 0.24                         |
|                   | 0.10/0.20/12      | $18.99 \pm 0.15$ | $-3.29 \pm 0.17$ | 0.17                         | $-2.84 \pm 0.19$ | $15.71 \pm 0.18$ | 0.18                         |
|                   | 0.20/0.10/15      | $25.18 \pm 0.14$ | $-2.31 \pm 0.10$ | 0.09                         | $-2.34 \pm 0.12$ | $7.44 \pm 0.09$  | 0.31                         |
|                   | 0.10/0.30/10      | $33.14 \pm 0.44$ | $-8.28 \pm 0.39$ | 0.25                         | $-9.25 \pm 0.46$ | $39.11 \pm 0.40$ | 0.24                         |
| $d_1:d_2 = 1:4$   | 0.10/0.10/20      | $12.36 \pm 0.04$ | $-0.74 \pm 0.04$ | 0.06                         | $-0.74 \pm 0.04$ | $3.37 \pm 0.03$  | 0.22                         |
|                   | 0.10/0.20/14      | $24.01 \pm 0.18$ | $-3.12 \pm 0.15$ | 0.13                         | $-3.09 \pm 0.19$ | $13.50 \pm 0.18$ | 0.23                         |
|                   | 0.20/0.10/24      | $26.56 \pm 0.06$ | $-1.85 \pm 0.05$ | 0.07                         | $1.85 \pm 0.06$  | $5.71 \pm 0.08$  | 0.32                         |
|                   | 0.10/0.30/14      | $40.69 \pm 0.45$ | $-8.62 \pm 0.64$ | 0.21                         | $-8.46 \pm 0.41$ | $35.51 \pm 0.68$ | 0.24                         |

The first column contains the volume fractions and the number of configurations; the second, third, fifth, and sixth columns contain the dimensionless volume-specific friction coefficient  $\beta_{ij}^*$ . The ratio of the off-diagonals to the diagonals in the fourth and last columns indicate the importance of the hydrodynamic particle–particle drag. In all simulations  $\lambda/d_1 = 0.05$ .

$-\beta_{21}^*/\beta_{22}^*$  representing the weight of the off-diagonals relative to the diagonals. It can be observed that the off-diagonals in the friction coefficient matrix are fairly significant compared to the diagonals, and they produce particle–particle drag forces that should not be neglected from the total fluid-particle drag force.

It may be observed from the data that the ratio  $-\beta_{12}^*/\beta_{11}^*$  decreases with increasing particle size difference, and the ratio  $-\beta_{21}^*/\beta_{22}^*$  increases with increasing particle size difference. These opposing trends, which are most obvious between the data obtained with  $d_1:d_2 = 1:1.5$  and those with  $d_1:d_2 = 1:4$ , can be explained as smaller particles would have fewer larger particle neighbors if the size difference between species increases, whereas the larger particles on average would find more smaller particles neighbors under the same situation. In addition, similar to what was reported in Yin and Sundaresan,<sup>18</sup> the off-diagonals decrease with increasing lubrication cutoff distance, indicating that the lubrication interaction between particles provides important contributions to the hydrodynamic particle–particle drag.

When we look for functions to fit  $\beta_{ij}^*$ , it is useful to recognize that the four components in  $\beta_{ij}^*$  are not independent of each other. Based on the principle of action and reaction between particle species,  $\beta_{ij}^*$  should always be symmetric, i.e.,  $\beta_{12}^* = \beta_{21}^*$ . In addition, in order to reproduce the friction

coefficients of bidisperse fixed beds when  $\Delta U_1 = \Delta U_2$ ,  $\beta_{ij}^*$  must satisfy two constraints

$$\begin{aligned} \beta_{11}^* + \beta_{12}^* &= \beta_1^* \\ \beta_{21}^* + \beta_{22}^* &= \beta_2^* \end{aligned} \quad (42)$$

where  $\beta_i^* = \beta_i \langle d \rangle^2 / \mu$  is the dimensionless form of  $\beta_i$  that is related to  $F_{Di}^*$  by Eq. 13. Our simulation data listed in Table 2 through Table 5 indicate that  $\beta_{ij}^*$  are indeed roughly symmetric. As shown in the left panel of Figure 6,  $\beta_{12}^*/\beta_{21}^*$  as a function of  $\phi$  were always close to unity. In the right panel of Figure 6, we show that the values of  $(\beta_{11}^* + \beta_{12}^*)/\beta_1^*$  and  $(\beta_{21}^* + \beta_{22}^*)/\beta_2^*$ , where  $\beta_1^*$  and  $\beta_2^*$  were obtained from our fixed-bed simulations [c.f. Table 1], were also close to unity. Because of these constraints, the friction coefficient matrix can be written into the following form where  $\beta_{12}^*$  is the only free parameter

$$\begin{bmatrix} \beta_{11}^* & \beta_{12}^* \\ \beta_{21}^* & \beta_{22}^* \end{bmatrix} = \begin{bmatrix} \beta_1^* - \beta_{12}^* & \beta_{12}^* \\ \beta_{12}^* & \beta_2^* - \beta_{12}^* \end{bmatrix}. \quad (43)$$

Since we have already developed accurate fitting functions for  $\beta_1^*$  and  $\beta_2^*$  [Eqs. 23 and 25], it is our next task to look for appropriate functions to account for the dependence of  $\beta_{12}^*$  on  $\phi_i$ ,  $d_i$ , and  $\lambda$ .

**Table 5. List of Polydisperse Suspension Simulations with Particle–Particle Relative Motions**

| Size Ratio        | $\phi_1/\phi_2/M$ | $\beta_{11}^*$   | $\beta_{12}^*$   | $-\beta_{12}^*/\beta_{11}^*$ | $\beta_{21}^*$   | $\beta_{22}^*$   | $-\beta_{21}^*/\beta_{22}^*$ |
|-------------------|-------------------|------------------|------------------|------------------------------|------------------|------------------|------------------------------|
| $d_1:d_2 = 1:1.5$ | 0.10/0.10/14      | $8.40 \pm 0.07$  | $-0.71 \pm 0.04$ | 0.08                         | $-0.71 \pm 0.06$ | $5.50 \pm 0.04$  | 0.13                         |
|                   | 0.10/0.20/12      | $13.88 \pm 0.11$ | $-2.34 \pm 0.09$ | 0.17                         | $-2.17 \pm 0.13$ | $17.62 \pm 0.10$ | 0.12                         |
|                   | 0.20/0.10/15      | $21.91 \pm 0.06$ | $-1.87 \pm 0.08$ | 0.08                         | $-2.00 \pm 0.07$ | $8.62 \pm 0.08$  | 0.23                         |
|                   | 0.10/0.30/12      | $23.37 \pm 0.09$ | $-5.95 \pm 0.37$ | 0.25                         | $-6.74 \pm 0.36$ | $40.80 \pm 0.40$ | 0.16                         |
| $d_1:d_2 = 1:2.5$ | 0.10/0.10/13      | $10.71 \pm 0.12$ | $-0.94 \pm 0.13$ | 0.09                         | $-0.94 \pm 0.12$ | $4.45 \pm 0.12$  | 0.21                         |
|                   | 0.10/0.20/12      | $18.49 \pm 0.08$ | $-2.65 \pm 0.13$ | 0.14                         | $-2.34 \pm 0.14$ | $15.07 \pm 0.14$ | 0.16                         |
|                   | 0.20/0.10/15      | $24.72 \pm 0.12$ | $-1.83 \pm 0.07$ | 0.07                         | $-1.87 \pm 0.09$ | $6.97 \pm 0.07$  | 0.27                         |
|                   | 0.10/0.30/10      | $31.43 \pm 0.34$ | $-6.74 \pm 0.35$ | 0.21                         | $-7.55 \pm 0.35$ | $37.56 \pm 0.36$ | 0.20                         |
| $d_1:d_2 = 1:4$   | 0.10/0.10/20      | $12.24 \pm 0.03$ | $-0.59 \pm 0.04$ | 0.05                         | $-0.62 \pm 0.03$ | $3.23 \pm 0.03$  | 0.19                         |
|                   | 0.10/0.20/14      | $23.40 \pm 0.14$ | $-2.54 \pm 0.12$ | 0.11                         | $-2.47 \pm 0.16$ | $12.92 \pm 0.16$ | 0.19                         |
|                   | 0.20/0.10/24      | $26.26 \pm 0.05$ | $-1.55 \pm 0.05$ | 0.06                         | $-1.54 \pm 0.05$ | $5.40 \pm 0.08$  | 0.28                         |
|                   | 0.10/0.30/14      | $39.26 \pm 0.40$ | $-7.11 \pm 0.56$ | 0.18                         | $-7.08 \pm 0.38$ | $34.01 \pm 0.61$ | 0.21                         |

The first column contains the volume fractions and the number of configurations; the second, third, fifth, and sixth columns contain the dimensionless volume-specific friction coefficient  $\beta_{ij}^*$ . The ratio of the off-diagonals to the diagonals in the fourth and last columns indicate the importance of the hydrodynamic particle–particle drag. In all simulations  $\lambda/d_1 = 0.1$ .

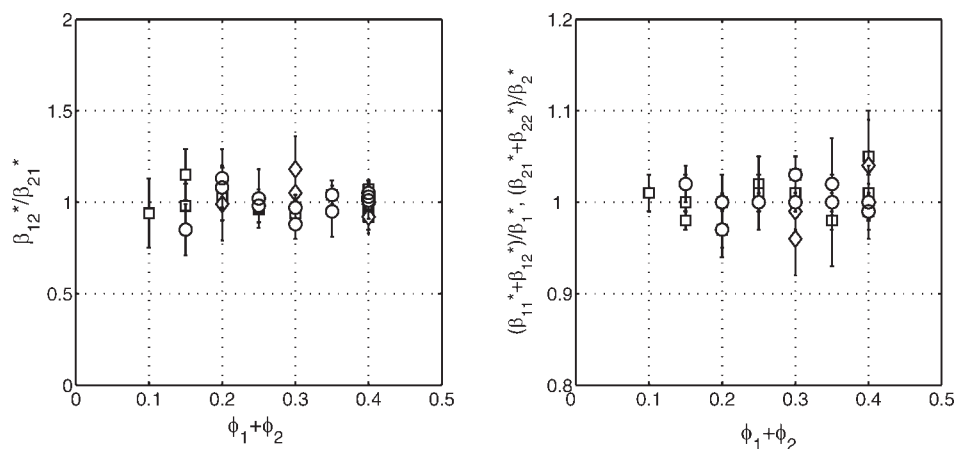


**Figure 6.** The left panel shows  $\beta_{12}^*/\beta_{21}^*$  as a function of total volume fraction  $\phi = \phi_1 + \phi_2$ ; the right panel shows the values of  $(\beta_{11}^* + \beta_{12}^*)/\beta_1^*$  and  $(\beta_{21}^* + \beta_{22}^*)/\beta_2^*$  as a function of  $\phi$ .

The squares, diamonds, and circles represent simulation data with  $d_1:d_2 = 1:1.5, 1:2.5,$  and  $1:4,$  respectively. The lubrication cutoff  $\lambda/d_1 = 0.001$ . This figure indicates that (1) the volume-specific friction coefficient matrix  $\beta_{ij}^*$  is nearly symmetric, and (2) the row summation of  $\beta_{ij}^*$  recovers the friction coefficients in bidisperse fixed beds of the particle composition. The error bars represent 90% confidence intervals due to variations in particle configurations.

In the process of seeking fitting functions for  $\beta_{12}^*$ , we were assisted by the insight gained from our previous study on polydisperse suspensions containing equally sized spheres.<sup>18</sup> In that study, it was found that for the special case of  $d_1 = d_2 = d$ , the friction coefficient matrix is simply

$$\begin{bmatrix} \beta_{11}^* & \beta_{12}^* \\ \beta_{21}^* & \beta_{22}^* \end{bmatrix} = 18(1 - \phi)F_{D\text{-fixed}}^* \begin{bmatrix} (1 + \alpha\phi_2)\phi_1 & -\alpha\phi_1\phi_2 \\ -\alpha\phi_1\phi_2 & (1 + \alpha\phi_1)\phi_2 \end{bmatrix}, \quad (44)$$

where  $\alpha$  is a logarithmic function of the distance on which the lubrication force between particles begins to saturate

$$\alpha = 1.313 \log_{10}(d/\lambda) - 1.249, \quad (45)$$

and  $F_{D\text{-fixed}}^*$  is the dimensionless drag of a monodisperse fixed bed of the same volume fraction [c.f. Eq. 7]. Comparing Eq. 44 with Eq. 43, one can see that for the case of  $d_1 = d_2 = d$ ,  $\beta_{12}^*$  is proportional to  $\beta_1^*$  and  $\beta_2^*$

$$\frac{\beta_{12}^*}{\phi_1\phi_2} = -\alpha \frac{\beta_1^*}{\phi_1} = -\alpha \frac{\beta_2^*}{\phi_2}. \quad (46)$$

Motivated by Eq. 46, we sought functions to relate  $-\beta_{12}^*/\phi_1\phi_2$  to  $\beta_1^*/\phi_1$  and  $\beta_2^*/\phi_2$ . Such functions should only contain symmetric combinations of  $\beta_1^*/\phi_1$  and  $\beta_2^*/\phi_2$ , e.g.,  $\beta_1^*/\phi_1 + \beta_2^*/\phi_2$  or  $\beta_1^*\beta_2^*/\phi_1\phi_2$ , because a drag law should not depend on the way in which the particle species are indexed. After experimenting several different ways of combining  $\beta_1^*/\phi_1$  and  $\beta_2^*/\phi_2$ , we found that  $-\beta_{12}^*/\phi_1\phi_2$  can be approximated by a linear function of the harmonic mean of  $\beta_1^*/\phi_1$  and  $\beta_2^*/\phi_2$

$$\frac{\beta_{12}^*}{\phi_1\phi_2} = -\alpha \frac{2}{\phi_1/\beta_1^* + \phi_2/\beta_2^*}, \quad (47)$$

where  $\alpha$  is given by

$$\alpha = 1.313 \log_{10}(d_1/\lambda) - 1.249. \quad (48)$$

In Eq. 48, we used  $d_1$ , the size of the smaller particle species, to normalize  $\lambda$ . Eqs. 47 and 48 are reduced to Eqs. 46 and 45 for the special case of  $d_1 = d_2$  and  $\beta_1^*/\phi_1 = \beta_2^*/\phi_2$ .

As Figure 7 shows, the expressions Eqs. 47 and 48 (the solid lines) provide good fittings for all  $\beta_{12}^*$  characterized from our numerical simulations (the symbols) regardless of volume fractions and particle size ratios. The average percentage deviation from Eqs. 47 and 48 with  $\beta_1^*$  and  $\beta_2^*$  determined from Eq. 27 to the numerical data is 13%; the maximum deviation is 31%. It may be observed from Figure 7 that most of the data points fall into the range of  $\pm 13\%$  from the predictions of Eqs. 47 and 48 between the dashed lines sandwiching the center solid lines.

The fact that  $-\beta_{12}^*/\phi_1\phi_2$  can be approximated by the product of a logarithmic function of  $\lambda/d_1$  and the harmonic mean of  $\beta_1^*/\phi_1$  and  $\beta_2^*/\phi_2$ , again, shows the importance of the local lubrication interactions between particles in the overall hydrodynamic particle-particle drag. In a random bidisperse suspension, the probability of finding a particle of species 2 right next to a particle of species 1—the probability of mutual contact—is known to be proportional to the harmonic mean of the two particle sizes.<sup>45</sup> As the overall lubrication force between particle species is proportional to the probability of mutual contact, it is not surprising that  $-\beta_{12}^*/\phi_1\phi_2$  appeared to be proportional to the harmonic mean of  $\beta_1^*/\phi_1$  and  $\beta_2^*/\phi_2$ . In fact, it was the above chain of thoughts that led us to Eq. 47, which turned out to be a simple yet excellent fitting function for our simulation data at all volume fractions and particle size ratios.

Equations 47 and 48 can easily be generalized to suspensions containing three or more species moving with different velocities relative to the fluid

$$\beta_{ij}^* = -\frac{2\alpha_{ij}\phi_i\phi_j}{\phi_i/\beta_i^* + \phi_j/\beta_j^*}. \quad (49)$$

In the above equation,  $\alpha_{ij}$  is a logarithmic function of the ratio between the lubrication cutoff  $\lambda$  and the size of the smaller particle species of the two

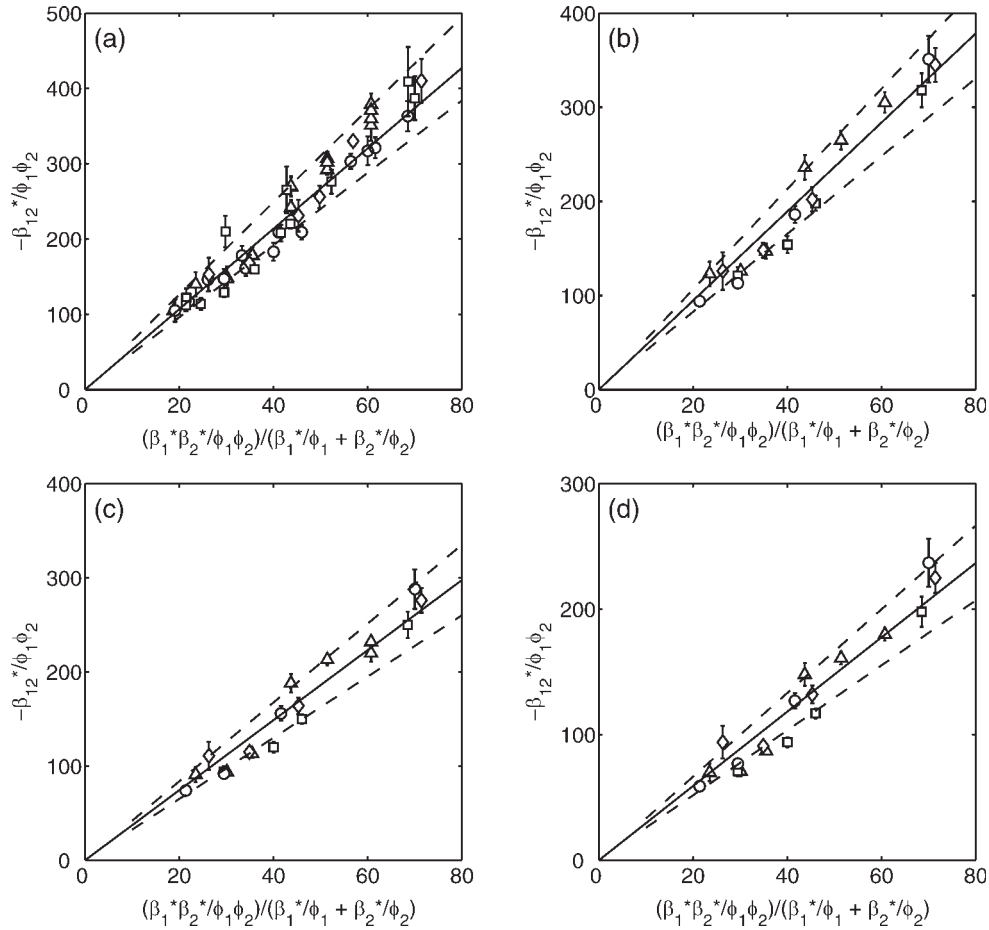


**Figure 7.** This figure shows the approximate linear dependence of  $-\beta_{12}^*/\phi_1\phi_2$  on the harmonic mean of  $\beta_1^*/\phi_1$  and  $\beta_2^*/\phi_2$  for four different values of the lubrication cutoff: (a)  $\lambda/d_1 = 0.001$ , (b)  $\lambda/d_1 = 0.002$ , (c)  $\lambda/d_1 = 0.005$ , (d)  $\lambda/d_1 = 0.01$ .

The squares, diamonds, and circles represent, respectively, simulation data with  $d_1:d_2 = 1:1.5, 1:2.5, \text{ and } 1:4$ . The upward triangles correspond to data from Yin and Sundaresan<sup>18</sup> where  $d_1 = d_2$ . The solid lines are based on the proposed fitting function Eq. 47 with  $\alpha$  given by Eq. 48; the dashed lines represent the  $\pm 13\%$  range of average deviations. The error bars represent 90% confidence intervals due to variations in particle configurations.

$$\alpha_{ij} = 1.313 \log_{10}(\min(d_i, d_j)/\lambda) - 1.249. \quad (50)$$

The net fluid-particle drag force per volume of suspension acting on species  $i$  is therefore

$$\begin{aligned} f_{Di}^* &= -\beta_i^* \Delta \text{Re}_i - \sum_{j \neq i} \beta_{ij}^* (\Delta \text{Re}_j - \Delta \text{Re}_i) \\ &= -\beta_i^* \Delta \text{Re}_i - \sum_{j \neq i} \frac{2\alpha_{ij} \phi_i \phi_j}{\phi_i/\beta_i^* + \phi_j/\beta_j^*} (\Delta \text{Re}_i - \Delta \text{Re}_j). \end{aligned} \quad (51)$$

One can substitute

$$\beta_i^* = \frac{18\phi_i(1-\phi)}{y_i^2} F_{Di}^* \text{-fixed} \quad (52)$$

and

$$F_{Di}^* = \frac{\pi y_i^3}{6\phi_i} f_{Di}^* \quad (53)$$

into Eq. 51 to obtain the expression for the average fluid-particle drag per particle

$$\begin{aligned} F_{Di}^* &= -3\pi(1-\phi) \\ &\times \left[ y_i \Delta \text{Re}_i F_{Di}^* \text{-fixed} + \sum_{j \neq i} \frac{2\alpha_{ij} \phi_j y_i^3 (\Delta \text{Re}_i - \Delta \text{Re}_j)}{y_i^2 / F_{Di}^* \text{-fixed} + y_j^2 / F_{Dj}^* \text{-fixed}} \right]. \end{aligned} \quad (54)$$

We constructed two ternary suspensions to test the applicability of Eq. 51 to general polydisperse gas–solid suspensions. Table 6 lists the volume fractions, sizes, and velocities of different particle species. It can be observed that the dimensionless drag forces calculated from Eq. 51 are very close to the actual drag forces obtained from simulations. Table 6 also shows that neglecting particle–particle hydrodynamic drag terms by setting  $\alpha_{ij}$  to zero in Eq. 51 increases the differences between the calculated drag forces and the simulation data, proving that drag laws including hydrodynamic particle–particle drag terms are more accurate than the drag laws without such terms.

**Table 6. Verification of the Drag Law Eq. 51 for Two Ternary Suspensions**

|                                      | Suspension #1  | Suspension #2  |
|--------------------------------------|--|--|
| $\phi_{1,2,3}$                       | 0.07 / 0.07 / 0.07                                       | 0.02 / 0.085 / 0.03  |
| $d_{1,2,3}(\Delta x)$                | 9.60 / 12.0 / 14.4                                       | 7.60 / 9.60 / 11.6   |
| $N_{1,2,3}$                          | 510 / 261 / 151  | 84 / 180 / 36  |
| $M$                                  | 20   | 19   |
| $\langle d \rangle (\Delta x)$       | 11.7   | 9.60   |
| $\Delta \text{Re}_{1,2,3}$           | 0.0346 / 0.0485 / 0.0653                                 | 0.0252 / 0.0372 / 0.0466                                       |
| $f_{D1,2,3}^*$ (simulation)          | $-0.085 \pm 0.001 / -0.104 \pm 0.001 / -0.133 \pm 0.001$ | $-0.0143 \pm 0.0004 / -0.0686 \pm 0.0004 / -0.0311 \pm 0.0004$ |
| $f_{D1,2,3}^*$ (Eq. 50)              | -0.083 / -0.103 / -0.127                                 | -0.0132 / -0.0721 / -0.0315                                    |
| $f_{D1,2,3}^*$ ( $\alpha_{ij} = 0$ ) | -0.095 / -0.103 / -0.115                                 | -0.0155 / -0.0728 / -0.0285                                    |

Rows 1–4 contain the volume fractions, particle sizes in terms of lattice spacing  $\Delta x$ , numbers of particles in each simulation, and number of configurations. The fifth row contains the Sauter mean of the two suspensions, from which the Reynolds numbers in the sixth row were calculated. The last three rows compare the dimensionless drag forces obtained from simulations (the numbers after  $\pm$  sign represent the 90% uncertainty levels) to those based on Eq. 51 using  $\lambda = 0.01\Delta x$ , and those based on Eq. 51 assuming zero hydrodynamic particle–particle drag ( $\alpha_{ij} = 0$ ).

## Summary

Using the lattice-Boltzmann method, we characterized the fluid-particle drag forces in low-Reynolds-number bidisperse fixed beds and gas–solid suspensions with particle–particle relative motions. These particles are spherical in shape, and they are intimately mixed (the microstructure of our bidisperse suspensions is identical to that of a binary hard sphere fluid) and are assumed to have moderate-to-high Stokes numbers such that their fluctuating motions are not much affected by the hydrodynamic forces between successive collisions. This low-Re, high-St dual limit is realistic for many gas–solid suspensions containing 50–100  $\mu\text{m}$  size particles under typical pressure conditions, and it allows for efficient characterization of the drag forces and the friction coefficients due to the linearity of the system.

For bidisperse fixed beds, our numerical data in the volume fraction range of  $0.1 < \phi < 0.4$  agree very well with the existing data by van der Hoef et al.<sup>8,9</sup> Our data showed that the previously developed drag law by van der Hoef et al.,<sup>8,9</sup> for fixed beds is only accurate when the size difference between particles is moderate; in fixed beds with large size differences (1:4), our data confirmed that there is a systematic difference. By analyzing the general trend of existing data (both ours and those in van der Hoef et al.<sup>8,9</sup>) and the limiting behaviors of the drag forces, we developed a modified drag formula for polydisperse fixed beds

$$F_{Di-\text{fixed}}^* = \frac{1}{1-\phi} + \left( F_{D-\text{fixed}}^* - \frac{1}{1-\phi} \right) [ay_i + (1-a)y_i^2],$$

where  $a$  is a cubic polynomial of the total volume fraction of the suspension

$$a(\phi) = 1 - 2.660\phi + 9.096\phi^2 - 11.338\phi^3,$$

$F_{Di-\text{fixed}}^*$  is the dimensionless drag force per particle of type  $i$  in a polydisperse fixed bed [c.f. Eq. 10],  $F_{D-\text{fixed}}^*$  is the dimensionless drag force in a monodisperse fixed bed [c.f. Eq. 7], and  $y_i$  is the dimensionless particle size ratio  $d_i/\langle d \rangle$  with  $\langle d \rangle$  the Sauter mean of the suspension [c.f. Eq. 26]. In the volume fraction range  $0.1 < \phi < 0.5$ , this new drag law fits the existing numerical data with an average percentage error of 3.9% and a maximum error of 9.4%; thus, it is a significant improvement over the existing drag formulas. On the basis of this drag formula, a relation between the overall pressure drop

$dP/dx$  for a porous medium with a continuous grain size distribution  $\sigma(d)$  and the superficial fluid velocity  $U_s$  through the medium is developed

$$\frac{dP}{dx} = -\frac{18\phi\mu U_s}{(1-\phi)\langle d \rangle^2} \left[ F_{D-\text{fixed}}^* + \frac{1}{1-\phi} \left( \frac{\sigma_I\sigma_{III}}{\sigma_{II}\sigma_{II}} - 1 \right) \right],$$

where  $\sigma_I$ ,  $\sigma_{II}$ , and  $\sigma_{III}$  are the first, second, and third order moments of  $\sigma(d)$ , and  $\langle d \rangle = \sigma_{III}/\sigma_{II}$ .

For bidisperse gas–solid suspensions with particle–particle relative motions, our objective is to characterize and develop fitting functions for the hydrodynamic particle–particle drag, a term that is not very well understood to date and is usually neglected in the existing drag formulas. Because of the linearity of low-Re flows, the drag forces acting on the two particle species in a bidisperse suspension with particle–particle relative motion may be expressed as linear functions of their respective velocities relative to the fluid. The proportionality constants between the forces and the velocities, known as the friction coefficients, is a matrix the off-diagonals of which are indicative of the size of the hydrodynamic particle–particle drag. Our numerical data for the friction coefficient matrix indicate that the off-diagonals produce sizeable contributions to the drag forces, and they are in fact linear functions of the harmonic means of the drags in bidisperse fixed beds [c.f. Eq. 49]. The net dimensionless fluid-particle drag force per volume of suspension acting on particles of type  $i$  in a polydisperse suspension where different particle types have different velocities relative to the fluid is

$$f_{Di}^* = -\beta_i^* \Delta \text{Re}_i - \sum_{j \neq i} \frac{2\alpha_{ij}\phi_i\phi_j}{\phi_i/\beta_i^* + \phi_j/\beta_j^*} (\Delta \text{Re}_i - \Delta \text{Re}_j).$$

In the above equation,  $f_{Di}^*$  and  $\Delta \text{Re}_i$  are defined in Eq. 19,  $\beta_i^*$  is the volume-specific friction coefficient for type  $i$  particles in a polydisperse fixed bed of the same composition and is related to  $F_{Di-\text{fixed}}^*$  by Eq. 52, and  $\alpha_{ij}$  is a logarithmic function of the ratio between the lubrication cutoff  $\lambda$  and the size of the smaller particle species of the two

$$\alpha_{ij} = 1.313 \log_{10}(\min(d_i, d_j)/\lambda) - 1.249.$$

This drag formula fits our numerical data with an average percentage deviation of 13%, and a maximum deviation of

31%. The logarithmic dependence of the off-diagonals on the lubrication cutoff indicates that the hydrodynamic particle–particle drag in polydisperse suspensions of spherical particles of infinite Stokes numbers would diverge to infinity due to the strong lubrication interaction between close pairs of dissimilar particles. To suppress this nonphysical divergence, a length scale  $\lambda$  on which the lubrication force becomes saturated is needed—it reflects the reality that the growth of the lubrication force between two approaching particles would eventually be limited by surface roughness, non-continuum effects, or finite weights of the particles.

The difference between a freely evolving bidisperse suspension and a frozen bidisperse suspension is that the freely evolving suspension can develop instabilities, and the particle–particle momentum transfer will include an extra term due to direct collision and friction [c.f. Eq. 4]. In this study, we used frozen suspensions the microstructure of which is identical to that of a binary hard sphere suspension to isolate the particle–particle hydrodynamic momentum transfer under an idealized condition. Another study is underway to study the instability / microstructure and particle–particle collisional momentum transfer in high-St freely evolving binary suspensions. Allowing the particles to move also opens up possibilities to extend the formulas presented in this study to finite Reynolds number regime. Despite that binary gas–solid suspensions are usually unstable (e.g. see Valiveti and Koch<sup>46</sup>), as the instability is usually manifested on large length scales, we expect that our drag law will apply on sufficiently small differential volumes where segregation and nonrandom distribution of particles are not critically important and that this segregation should naturally emerge as an instability mode of the Euler-Euler model.

## Acknowledgements

This research received supports from ExxonMobil Corporation, US Department of Energy (DE-FC26-07NT43098), and ACS Petroleum Research Fund (43901-AC9). The authors would like to acknowledge graduate student William Holloway for assisting in the verification of the applicability of the drag laws to ternary fixed beds and suspensions, and Professor Jos Derksen for supplying us a bidisperse particle configuration generator.

## Literature Cited

- Leboreiro J, Joseph GG, Hrenya CM. Revisiting the standard drag law for bubbling, gas-fluidized beds. *Powder Tech.* 2008;183:385–400.
- Leboreiro J, Joseph GG, Hrenya CM, Snider DM, Banerjee SS, Galvin JE. The influence of binary drag laws on simulations of species segregation in gas-fluidized beds. *Powder Tech.* 2008;184:275–299.
- Bokkers GA, van Sint Annaland M, Kuipers JAM. Mixing and segregation in a bidisperse gas–solid fluidized bed: a numerical and experimental study. *Powder Tech.* 2004;140:176–186.
- Beetstra R, van der Hoef MA, Kuipers JAM. Numerical study of segregation using a new drag force correlation for polydisperse systems derived from lattice-Boltzmann simulations. *Chem Eng Sci.* 2007;62:246–255.
- Hill RJ, Koch DL, Ladd AJC. The first effects of fluid inertia on flows in ordered and random arrays of spheres. *J Fluid Mech.* 2001;448:213–241.
- Hill RJ, Koch DL, Ladd AJC. Moderate-Reynolds-number flows in ordered and random arrays of spheres. *J Fluid Mech.* 2001;448:243–278.
- Benyahia S, Syamlal M, O'Brien TJ. Extension of Hill-Koch-Ladd drag correlation over all ranges of Reynolds number and solid volume fraction. *Powder Tech.* 2006;162:166–174.
- van der Hoef MA, Beetstra R, Kuipers JAM. Lattice-Boltzmann simulations of low-Reynolds-number flow past mono- and bidisperse arrays of spheres. *J Fluid Mech.* 2005;528:233–254.
- van der Hoef MA. Erratum. *AIChE J.* 2007;53:3020.
- Beetstra R, van der Hoef MA, Kuipers JAM. Drag force of intermediate Reynolds number flows past mono- and bidisperse arrays of spheres. *AIChE J.* 2007;53:489–501.
- Wylie JJ, Koch DL. Rheology of suspensions with high particle inertia and moderate fluid inertia. *J Fluid Mech.* 2003;480:95–118.
- Khoe GK, Ip TL, Grace JR. Rheological and fluidization behavior of powders of different particle-size distribution. *Powder Tech.* 1991;66:127–141.
- Sun G, Grace JR. Effect of particle-size distribution in different fluidization regimes. *AIChE J.* 1992;38:716–722.
- Gauthier D, Zerguerras S, Flamant G. Influence of the particle size distribution of powders on the velocities of minimum and complete fluidization. *Chem Eng J.* 1999;74:181–196.
- Lin CL, Wey MY, You SD. The effect of particle size distribution on minimum fluidization velocity at high temperature. *Powder Tech.* 2002;126:297–301.
- Lorences MJ, Patience GS, Diez FV, Coca J. Fines effects on collapsing fluidized beds. *Powder Tech.* 2003;131:234–240.
- Shadle LJ, Spenik J, Sarra A, Ontko J. Factorial tests on process operating conditions and bed fines on the circulating fluid bed performance. *Ind Eng Chem Res.* 2004;43:4166–4173.
- Yin X, Sundaresan S. Drag law for bidisperse gas–solid suspensions containing equally sized spheres. *Ind Eng Chem Res.* 2009;42:227–241.
- Koch DL. Kinetic theory for a monodisperse gas–solid suspension. *Phys Fluids A.* 1990;2:1711–1723.
- Kumaran V, Koch DL. Properties of a bidisperse particle-gas suspension. Part 1. Collision time small compared to the viscous relaxation time. *J Fluid Mech.* 1993;247:623–641.
- Batchelor GK. Sedimentation in a dilute polydisperse system of interacting spheres. Part 1. General theory. *J Fluid Mech.* 1982;119:379–408.
- Batchelor GK, Wen CS. Sedimentation in a dilute polydisperse system of interacting spheres. Part 2. Numerical results. *J Fluid Mech.* 1982;124:495–528.
- Davis RH, Gecol H. Hindered settling function with no empirical parameters for polydisperse suspensions. *AIChE J.* 1994;40:570–575.
- Revay JM, Higdon JLL. Numerical simulation of polydisperse sedimentation: equal size spheres. *J Fluid Mech.* 1992;243:15–32.
- Jackson R. Locally averaged equations of motion for a mixture of identical spherical particles and a Newtonian fluid. *Chem Eng Sci.* 1997;52:2457–2469.
- Syamlal M, Roger WA, O'Brien TJ. MFI documentation and theory guide. US Department of Energy: Technical Report DOE/METC94/1004, NTIS/DE94000087, 1993.
- Owoyemi O, Mazzei L, Lettieri P. CFD modeling of binary-fluidized suspensions and investigation of role of particle–particle drag on mixing and segregation. *AIChE J.* 2007;53:1924–1940.
- Feng YQ, Xu BH, Zhang SJ, Yu AB. Discrete particle simulation of gas fluidization of particle mixtures. *AIChE J.* 2004;50:1713–1728.
- Snider DM. An incompressible three-dimensional multiphase particle-in-cell model for dense particle flows. *J Comp Phys.* 2001;170:523–549.
- Koch DL, Hill RJ. Inertial effects in suspensions and porous media flows. *Annu Rev Fluid Mech.* 2001;33:619–647.
- van Wachem BGM, Schouten JC, van den Bleek, CM, Krishna R, Sinclair JL. CFD modeling of gas-fluidized beds with a bimodal particle mixture. *AIChE J.* 2001;47:1292–1302.
- Huilin L, Yurong H, Gidaspo D, Lidan Y, Yukun Q. Size segregation of binary mixture of solids in bubbling fluidized beds. *Powder Tech.* 2003;134:86–97.
- Fan R, Marchisio DL, Fox RO. Application of the direct quadrature method of moments to polydisperse gas–solid fluidized beds. *Powder Tech.* 2004;139:7–20.
- Gera D, Syamlal M, O'Brien TJ. Hydrodynamics of particle segregation in fluidized beds. *Int J Multiphase Flow.* 2004;30:419–428.
- Cooper S, Coronella CJ. CFD simulations of particle mixing in a binary fluidized bed. *Powder Tech.* 2005;151:27–36.
- Dahl SR, Hrenya CM. Size segregation in gas–solid fluidized beds with continuous size distributions. *Chem Eng Sci.* 2005;60:6658–6673.

37. Syamlal M. The particle–particle drag term in a multiparticle model of fluidization. US Department of Energy: Technical Report DOE/MC/21353–2373, NTIS/DE87006500, 1987.
38. Huilin L, Gidaspow D, Manger E. Kinetic theory of fluidized binary granular mixtures. *Phys Rev E*. 2001;64:061301.
39. Ladd AJC. Numerical simulations of particulate suspensions via a discretized Boltzmann equation. Part 1. Theoretical foundation. *J Fluid Mech*. 1994;271:285–309.
40. Ladd AJC. Numerical simulations of particulate suspensions via a discretized Boltzmann equation. Part 2. Numerical results. *J Fluid Mech*. 1994;271:311–339.
41. Ladd AJC, Verberg R. Lattice-Boltzmann simulations of particle-fluid suspensions. *J Stat Phys*. 2001;104:1191–1251.
42. Nguyen NQ, Ladd AJC. Lubrication corrections for lattice-Boltzmann simulations of particle suspensions. *Phys Rev E*. 2002;66:046708.
43. Kim S, Karrila SJ. *Microhydrodynamics: Principles and Selected Applications*. New York: Dover, 2005.
44. Ashcroft NW, Langreth DC. Structure of binary liquid mixtures. I. *Phys Rev*. 1967;156:685–692.
45. Lebowitz JL. Exact solution of generalized Percus-Yevick equation for a mixture of hard spheres. *Phys Rev A*. 1964;133:895–899.
46. Valiveti P, Koch DL. The inhomogeneous structure of a bidisperse sedimenting gas–solid suspension. *Phys Fluids*. 1999;11:3283–3305.

Manuscript received Sept. 7, 2008, and revision received Nov. 15, 2008.